

Vortex lattices in binary Bose–Einstein condensates: collective modes, quantum fluctuations, and intercomponent entanglement

Takumi Yoshino^{1,*}, Shunsuke Furukawa^{2,*}  and Masahito Ueda^{1,3,4} 

¹ Department of Physics, University of Tokyo, 7-3-1 Hongo, Bunkyo-ku, Tokyo 113-0033, Japan

² Department of Physics, Keio University, 3-14-1 Hiyoshi, Kohoku-ku, Yokohama 223-8522, Japan

³ RIKEN Center for Emergent Matter Science (CEMS), Wako, Saitama 351-0198, Japan

⁴ Institute for Physics of Intelligence, University of Tokyo, 7-3-1 Hongo, Bunkyo-ku, Tokyo 113-0033, Japan

E-mail: yoshino@cat.phys.s.u-tokyo.ac.jp and furukawa@rk.phys.keio.ac.jp

Received 15 January 2022

Accepted for publication 19 April 2022

Published 20 May 2022



Abstract

We study binary Bose–Einstein condensates subject to synthetic magnetic fields in mutually parallel or antiparallel directions. Within the mean-field theory, the two types of fields have been shown to give the same vortex-lattice phase diagram. We develop an improved effective field theory to study properties of collective modes and ground-state intercomponent entanglement. Here, we point out the need to introduce renormalized coupling constants for coarse-grained densities. We show that the low-energy excitation spectra for the two types of fields are related to each other by suitable rescaling with the renormalized coupling constants. By calculating the entanglement entropy, we find that for an intercomponent repulsion (attraction), the two components are more strongly entangled in the case of parallel (antiparallel) fields, in qualitative agreement with recent studies for a quantum (spin) Hall regime. We also find that the entanglement spectrum exhibits an anomalous square-root dispersion relation, which leads to a subleading logarithmic term in the entanglement entropy. All of these are confirmed by numerical calculations based on the Bogoliubov theory with the lowest-Landau-level approximation. Finally, we investigate the effects of quantum fluctuations on the phase diagrams by calculating the correction to the ground-state energy due to zero-point fluctuations in the Bogoliubov theory. We find that the boundaries between rhombic-, square-, and rectangular-lattice phases shift appreciably with a decrease in the filling factor.

Keywords: multicomponent Bose–Einstein condensates, synthetic gauge fields, vortex lattices, quantum entanglement

(Some figures may appear in colour only in the online journal)

* Authors to whom any correspondence should be addressed.

 Original content from this work may be used under the terms of the [Creative Commons Attribution 4.0 licence](https://creativecommons.org/licenses/by/4.0/). Any further distribution of this work must maintain attribution to the author(s) and the title of the work, journal citation and DOI.

1. Introduction

Engineering synthetic gauge fields and observing their physical effects in ultracold atomic gases have been a subject of great interest in recent years [1–5]. While atomic gases are charge neutral, effective gauge fields can be induced by rotating gases [6, 7] or optically dressing atoms [8]. Atomic Bose–Einstein condensates (BECs) in synthetic magnetic fields have close analogy with type-II superconductors in magnetic fields. Both real and synthetic magnetic fields induce quantized vortices in these systems; when vortices proliferate in high fields, they form a regular lattice pattern owing to their repulsion, as originally predicted by Abrikosov [9]. The resulting triangular vortex lattice structure has been observed experimentally in rapidly rotating BECs [10–12]. A vortex lattice exhibits elliptically polarized oscillations known as the Tkachenko mode [13–16], which has also been observed in a trapped BEC [12, 17]. In a uniform system, the Tkachenko mode has a quadratic dispersion relation at low frequencies [18–22], and is understood as a Nambu–Goldstone mode associated with spontaneously broken U(1) symmetry and magnetic translation symmetries [23]. For sufficiently high synthetic magnetic fields, atoms are expected to be in the lowest Landau level (LLL). A key parameter in this regime is the filling factor $\nu := N/N_v$, where N is the number of atoms and N_v is the number of flux quanta piercing the system. While the Gross–Pitaevskii (GP) mean-field theory is applicable for $\nu \gg 1$ [24], quantum fluctuations become significant as ν is lowered [18, 20–22, 25]. Theory predicts that when ν is below a critical value ν_c , the vortex lattice melts and incompressible quantum Hall states appear at various integer and fractional values of ν [6, 26–28]. Estimates of ν_c vary over $\nu_c \simeq 2–6$ from exact diagonalization [27, 29, 30] and $\nu_c \simeq 5–14$ from a Lindemann criterion [18, 20, 22, 27].

For binary (or pseudospin- $\frac{1}{2}$) BECs, which are populated in two hyperfine spin states of the same atomic species, a richer variety of synthetic gauge fields have been realized, such as a uniform magnetic field by rotation [31], and spin–orbit couplings [32–34] and pseudospin-dependent antiparallel magnetic fields [35] by optical dressing techniques. For binary BECs under rotation, GP mean-field calculations have revealed that five vortex-lattice phases appear as the ratio of the intercomponent coupling $g_{\uparrow\downarrow}$ to the intracomponent one $g > 0$ is varied (see figure 1) [36–39]. Square vortex lattices (figure 1(d)) have indeed been observed experimentally [31]. Meanwhile, a spin Hall effect due to pseudospin-dependent Lorentz forces has been observed in binary BECs in antiparallel magnetic fields [35]. For high antiparallel fields, theory predicts a rich phase diagram that consists of vortex lattices and (fractional) quantum spin Hall states [40–42]. Remarkably, *within* the GP mean-field theory, binary BECs in antiparallel magnetic fields exhibit the *same* vortex phase diagram as those in parallel magnetic fields (i.e., under rotation) [42]. This is because the GP energy functionals as well as the time-independent GP equations for the two systems are related to each other through the complex conjugation of the spin- \downarrow condensate wave function. It is interesting to further investigate similarities and differences between the two

systems. As the systems in parallel and antiparallel magnetic fields are closely related with bilayer quantum Hall systems [43] and quantum spin Hall systems [44], respectively, a comparative study of these systems can make a link between the two research fields. Such studies have been conducted on collective modes of vortex lattices [45, 46] and phase diagrams in a quantum (spin) Hall regime [42, 47–52].

Collective excitation spectra can be different between the parallel- and antiparallel-field cases as there is no obvious correspondence between the two cases for the time-dependent GP equations. Keçeli and Oktel [45] have calculated excitation spectra in binary BECs under rotation by using a hydrodynamic theory. In a previous work [46], we have conducted a comparative study of excitation modes in the parallel- and antiparallel-field cases by means of the Bogoliubov theory and an effective field theory. All the calculations in these works are based on the LLL approximation. For both types of fields and for all the lattice structures in figure 1, it is found that there appear two distinct modes, one with a quadratic dispersion relation and the other with a linear dispersion relation at low energies, which exhibit anisotropy reflecting the symmetry of each lattice structure. Furthermore, for overlapping triangular lattices (figure 1(a)), the low-energy spectra for the two types of fields are found to be related to each other by simple rescaling [46]. This indicates a nontrivial correspondence between the two types of fields in excitation properties. However, such rescaling relations do not hold for other lattices, which appears inconsistent with the effective field theory prediction. A more refined description of low-energy modes has remained an open issue.

Numerical studies on the quantum (spin) Hall regime with $\nu = O(1)$ have revealed that binary Bose gases in parallel and antiparallel synthetic magnetic fields exhibit markedly different phase diagrams [42, 47–52]. For parallel fields, product states of a pair of nearly uncorrelated quantum Hall states are robust against an intercomponent attraction $g_{\uparrow\downarrow} < 0$ and persist even when $|g_{\uparrow\downarrow}|$ is close to g [52]. Meanwhile, a variety of spin-singlet quantum Hall states with high intercomponent entanglement emerge for $g_{\uparrow\downarrow} \approx g$ [47–51]. For antiparallel fields, (fractional) quantum spin Hall states approximated by products of quantum Hall states with opposite chiralities are robust against an intercomponent repulsion $g_{\uparrow\downarrow} > 0$ [42]. The phase diagrams for the two types of fields thus exhibit opposite behavior in view of intercomponent entanglement. An interpretation of these results has been given in light of pseudopotential representations of interactions [52]. As there is no intercomponent entanglement in the GP mean-field theory valid for $\nu \gg 1$, it is interesting to investigate how the intercomponent entanglement arises in the two systems as ν is lowered from the mean-field regime.

In this paper, we present a detailed comparative study of vortex lattices of binary BECs in parallel and antiparallel fields concerning ground-state and excitation properties. We first formulate an improved effective field theory for such vortex lattices, and derive some properties of collective modes and ground-state intercomponent entanglement. Here, a major

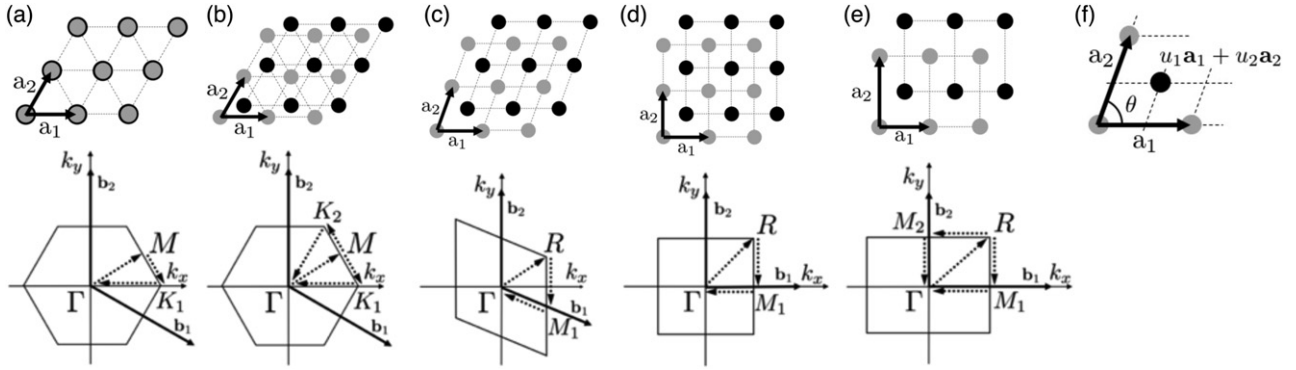


Figure 1. (Upper panels) Vortex-lattice structures in the ground state of the binary BECs under synthetic magnetic fields described by the Lagrangian in equation (1) [36–39] (see also references [53–59]). Within the GP mean-field theory, the systems in parallel and antiparallel fields exhibit the same phase diagrams [42]. Five different structures appear as the interaction ratio $g_{\uparrow\downarrow}/g$ is varied (see figure 10): (a) overlapping triangular lattices, (b) interlaced triangular lattices, (c) rhombic lattices, (d) square lattices, and (e) rectangular lattices. Black (grey) circles show the vortex positions of the spin- \uparrow (\downarrow) component. As shown in (f), each lattice structure is specified by the primitive vectors $\mathbf{a}_1 = (a, 0)$ and $\mathbf{a}_2 = b(\cos \theta, \sin \theta)$ as well as the vortex displacement $u_1\mathbf{a}_1 + u_2\mathbf{a}_2$ in one component relative to the other. The area of the unit cell is given by $(\mathbf{a}_1 \times \mathbf{a}_2)_z = ab \sin \theta = 2\pi l^2$. The angle θ and the aspect ratio b/a vary continuously in the rhombic- and rectangular-lattice phases, respectively, as shown later in figure 11. (Lower panels) The Brillouin zone for each lattice structure shown above. The vectors \mathbf{b}_1 and \mathbf{b}_2 show the reciprocal primitive vectors, while uppercase letters show high-symmetry points. The excitation spectra and the single-particle ES presented in figures 3, 4 and 7 are calculated along the dotted arrows.

improvement is the introduction of renormalized coupling constants for coarse-grained densities⁵. We show that the low-energy excitation spectra for the two types of fields are related to each other by suitable rescaling using the renormalized constants. Namely, the rescaling relations proposed in our previous work [46] must be modified using the renormalized constants. By calculating the entanglement entropy (EE), we find that for an intercomponent repulsion (attraction), the two components are more strongly entangled in the case of parallel (antiparallel) fields, in qualitative agreement with recent exact diagonalization results for a quantum (spin) Hall regime [42, 52]. As a by-product, we also find that the entanglement spectrum (ES) exhibits an anomalous square-root dispersion relation, and that the EE exhibits a volume-law scaling with a subleading logarithmic correction. This anomalous feature of the ES is associated with the emergence of a long-range interaction in terms of the density in the entanglement Hamiltonian. All these predictions are confirmed by numerical calculations based on the Bogoliubov theory with the LLL approximation. Finally, we investigate the effects of quantum fluctuations on the phase diagrams by calculating the Lee–Huang–Yang correction, which is a correction to the ground-state energy due to zero-point fluctuations in the Bogoliubov theory [60]. We find that the boundaries between rhombic-, square-, and rectangular-lattice phases shift appreciably with a decrease in ν . Here, the shift occurs more significantly for parallel fields.

Let us comment on the relation to another recent work of our own [61] concerning intercomponent ES and EE in binary BECs in d spatial dimensions in the absence of synthetic gauge fields. Here we employ effective field theory to show that the ES exhibits a gapless square-root dispersion relation in the presence of an intercomponent tunneling (a Rabi coupling) and a gapped dispersion relation in its absence (see also references [62, 63] for related results in two coupled Tomonaga–Luttinger liquids). In the present work, in contrast, the ES exhibits a square-root dispersion relation in the absence of an intercomponent tunneling in both cases of parallel and antiparallel fields. This qualitative distinction is related to the fact that binary BECs in parallel and antiparallel fields have a higher density of low-energy excitations and thus experience larger quantum fluctuations than those without synthetic gauge fields. References [61, 63] and the present paper demonstrate that a variety of long-range interactions can be emulated in a subsystem of multicomponent BECs that have only short-range interactions. We also note that the field-theoretical methods for investigating intercomponent entanglement in the present paper are closely analogous to those in references [61–63].

The rest of this paper is organized as follows. In section 2, we introduce the systems that we study in this paper, and formulate the low-energy effective field theory to analyze excitation spectra, intercomponent entanglement, and correlation functions. In section 3, we briefly review the Bogoliubov theory with the LLL approximation, which has been adapted to the present problem in reference [46], and then give the expressions of the intercomponent ES and EE. In section 4, we present numerical results based on the Bogoliubov theory. We confirm the field-theoretical predictions on the excitation spectra, the intercomponent entanglement, and the fraction of quantum depletion. Furthermore, we investigate the effects of quantum fluctuations on the ground-state phase diagrams. In

⁵ In the formulation of reference [46], the necessity of renormalization was not transparent. This was because we integrated out the density variables, before coarse graining, to obtain an effective Lagrangian for phase variables. In this paper, we keep both the phase and density variables in the Lagrangian, and perform coarse graining of both the variables simultaneously. The renormalization of density–density interactions can naturally be understood in this formulation. This formulation also allows us to move easily to the operator formalism, in which ground-state and excitation properties can be studied in an algebraic manner.

section 5, we present a summary of the present study and an outlook for future studies. In appendices, we describe some technical details of section 2.

2. Effective field theory

Effective field theory for a vortex lattice in a scalar BEC has been developed in references [18, 23, 64, 65]. In our previous work [46], we applied the formulation by Watanabe and Murayama [23] to binary BECs in parallel and antiparallel fields. For parallel fields, this approach was essentially equivalent to the hydrodynamic theory by Keçeli and Oktel [45]. Here, we formulate an improved effective field theory for binary BECs in parallel and antiparallel fields by introducing renormalized coupling constants $\bar{g}_{\alpha\beta}$ for coarse-grained densities. In doing so, we keep both the phase and density variables in the Lagrangian, rather than integrating out the density variables as in reference [46]. We then move to the operator formalism, and study excitation spectra, intercomponent entanglement, and correlation functions in an algebraic manner (see references [61–63] for analogous calculations in different systems).

2.1. Systems

We consider a system of 2D binary (pseudospin- $\frac{1}{2}$) BECs having two hyperfine spin states (labeled by $\alpha = \uparrow, \downarrow$) and subject to synthetic magnetic fields B_\uparrow and B_\downarrow in mutually parallel or antiparallel directions. The Lagrangian density of the system is given by

$$\mathcal{L} = \sum_{\alpha=\uparrow,\downarrow} \left[\frac{i\hbar}{2} (\psi_\alpha^* \dot{\psi}_\alpha - \dot{\psi}_\alpha^* \psi_\alpha) - \frac{1}{2M} |(-i\hbar\nabla - q\mathbf{A}_\alpha)\psi_\alpha|^2 \right] - \sum_{\alpha,\beta=\uparrow,\downarrow} \frac{g_{\alpha\beta}}{2} |\psi_\alpha|^2 |\psi_\beta|^2, \quad (1)$$

where $\psi_\alpha(\mathbf{r}, t)$ is the bosonic field for the spin- α component (with $\mathbf{r} = (x, y)$ being the 2D coordinate), and M and q are the mass and the fictitious charge of an atom. This fictitious charge specifies the coupling strength between atoms and the synthetic gauge fields. The gauge field $\mathbf{A}_\alpha(\mathbf{r})$ for spin- α bosons is given by

$$\mathbf{A}_\alpha = \frac{B_\alpha}{2} \mathbf{e}_z \times \mathbf{r} = \epsilon_\alpha \frac{B}{2} (-y, x), \quad (2)$$

where we assume $qB > 0$ and $\epsilon_\uparrow = \epsilon_\downarrow = 1$ ($\epsilon_\uparrow = -\epsilon_\downarrow = 1$) for parallel (antiparallel) fields. The number of magnetic flux quanta piercing each component is given by $N_v = qBA/(2\pi\hbar) = A/(2\pi\ell^2)$, where A is the area of the system and $\ell := \sqrt{\hbar/qB}$ is the magnetic length. In the Lagrangian (1), the numbers of spin- \uparrow and \downarrow atoms, N_\uparrow and N_\downarrow , are separately conserved. We introduce the total filling factor $\nu := N/N_v$, where $N := N_\uparrow + N_\downarrow$ is the total number of atoms.

We assume a contact interaction between atoms. For simplicity, we set $g_{\uparrow\uparrow} = g_{\downarrow\downarrow} \equiv g > |g_{\uparrow\downarrow}|$ and $N_\uparrow = N_\downarrow$ in the following. With these conditions, the system in parallel fields is invariant under the interchange of the two components, while

the system in antiparallel fields is invariant under time reversal. To apply the LLL approximation, we further assume that the scale of the interaction energy per atom, $|g_{\alpha\beta}|n$, is much smaller than the Landau-level spacing $\hbar\omega_c$. Here, $n := N_\uparrow/A = N_\downarrow/A$ is the average density of \uparrow or \downarrow atoms, and $\omega_c := qB/M$ is the cyclotron frequency.

2.2. Effective field theory

To obtain a low-energy effective field theory description, it is useful to rewrite the field as $\psi_\alpha = e^{-i\theta_\alpha} \sqrt{n_\alpha}$, where $n_\alpha(\mathbf{r}, t)$ and $\theta_\alpha(\mathbf{r}, t)$ are the density and phase variables, respectively. The Lagrangian density (1) is rewritten in terms of these variables as

$$\mathcal{L} = \sum_\alpha \left[\hbar n_\alpha \dot{\theta}_\alpha - \frac{n_\alpha}{2M} (\hbar \nabla \theta_\alpha + q\mathbf{A}_\alpha)^2 - \frac{\hbar^2 (\nabla n_\alpha)^2}{8n_\alpha M} \right] - \sum_{\alpha,\beta} \frac{g_{\alpha\beta}}{2} n_\alpha n_\beta. \quad (3)$$

In the presence of vortices, the phase variables $\{\theta_\alpha(\mathbf{r}, t)\}$ involve singularities. This motivates us to decompose θ_α into regular and singular contributions as $\theta_\alpha = \theta_{\text{reg},\alpha} + \theta_{\text{sing},\alpha}$. We also introduce the displacement $\mathbf{u}_\alpha(\mathbf{r}, t)$ of a vortex from the equilibrium position. The derivatives of the singular part $\theta_{\text{sing},\alpha}$ of the phase can be related to the displacement field \mathbf{u}_α as [23, 64]

$$\hbar \dot{\theta}_{\text{sing},\alpha} = -\frac{qB_\alpha}{2} (\mathbf{u}_\alpha \times \dot{\mathbf{u}}_\alpha)_z, \quad (4a)$$

$$\hbar \nabla \theta_{\text{sing},\alpha} + q\mathbf{A}_\alpha = qB_\alpha \mathbf{e}_z \times \mathbf{u}_\alpha - \frac{qB_\alpha}{2} \epsilon_{ij} u_\alpha^i \nabla u_\alpha^j, \quad (4b)$$

where ϵ_{ij} is an antisymmetric tensor with $\epsilon_{xy} = -\epsilon_{yx} = +1$. The displacement $\mathbf{u}_\alpha(\mathbf{r}, t)$ also results in a change in the elastic energy $\int d^2\mathbf{r} \mathcal{E}_{\text{el}}(\mathbf{u}_\alpha, \partial_i \mathbf{u}_\alpha)$, whose explicit form will be given in section 2.3. The Lagrangian density can then be expressed in terms of $\{\theta_{\text{reg},\alpha}, \mathbf{u}_\alpha, n_\alpha\}$ as

$$\mathcal{L} = \sum_\alpha \left[\hbar n_\alpha \dot{\theta}_{\text{reg},\alpha} - \frac{qB_\alpha n_\alpha}{2} (\mathbf{u}_\alpha \times \dot{\mathbf{u}}_\alpha)_z - \frac{n_\alpha}{2M} \left(\hbar \nabla \theta_{\text{reg},\alpha} + qB_\alpha \mathbf{e}_z \times \mathbf{u}_\alpha - \frac{qB_\alpha}{2} \epsilon_{ij} u_\alpha^i \nabla u_\alpha^j \right)^2 - \frac{\hbar^2 (\nabla n_\alpha)^2}{8n_\alpha M} \right] - \sum_{\alpha,\beta} \frac{\bar{g}_{\alpha\beta}}{2} n_\alpha n_\beta - \mathcal{E}_{\text{el}}. \quad (5)$$

Henceforth, we ignore the term $-\frac{qB_\alpha}{2} \epsilon_{ij} u_\alpha^i \nabla u_\alpha^j$ in the round brackets as it only gives more than quadratic contributions to \mathcal{L} in terms of $\nabla \theta_{\text{reg},\alpha}$ and \mathbf{u}_α . We also omit the subscript ‘reg’ in $\theta_{\text{reg},\alpha}$.

In the effective Lagrangian density (5), we have introduced renormalized coupling constants $\bar{g}_{\alpha\beta}$ with $\bar{g}_{\uparrow\uparrow} = \bar{g}_{\downarrow\downarrow} \equiv \bar{g}$ and $\bar{g}_{\uparrow\downarrow} = \bar{g}_{\downarrow\uparrow}$. The necessity of this renormalization has been overlooked in previous studies [45, 46] and can be explained as follows. The introduction of the vortex displacement fields $\{\mathbf{u}_\alpha(\mathbf{r}, t)\}$ necessarily involves the coarse graining of the theory. Namely, we smooth out details within the scale of the

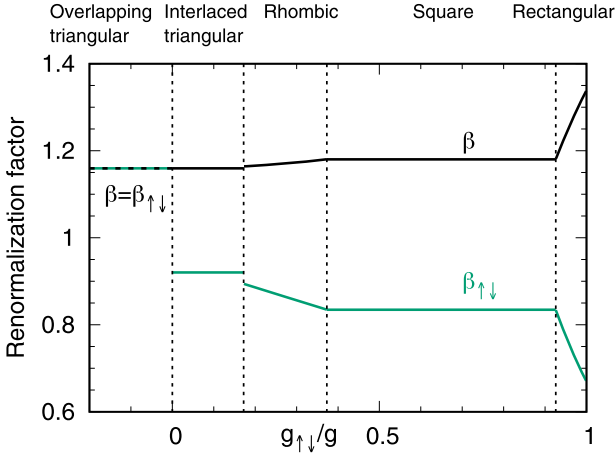


Figure 2. Renormalization factors $\beta := \bar{g}/g$ (black) and $\beta_{\uparrow\downarrow} := \bar{g}_{\uparrow\downarrow}/g_{\uparrow\downarrow}$ (green) for the intracomponent and intercomponent coupling constants. These factors are calculated using equation (83) for the mean-field vortex lattice structure for each $g_{\uparrow\downarrow}/g$, and take the same values for parallel and antiparallel fields. We set $N_v = 97^2$, with which a sufficient convergence to the thermodynamic limit is achieved. For overlapping triangular lattices ($-1 < g_{\uparrow\downarrow}/g < 0$), we have $\beta = \beta_{\uparrow\downarrow}$ and thus the two curves overlap; the value $\beta = \beta_{\uparrow\downarrow} = 1.1596$ in this region coincides with the renormalization factor obtained for a scalar BEC [7, 18, 66]. Vertical dashed lines indicate the transition points in the mean-field phase diagram [36].

lattice constants and instead focus on the physics at larger scales. Therefore, the density variable $n_{\alpha}(\mathbf{r}, t)$ should now be understood as the density averaged over the unit cell containing \mathbf{r} . The renormalized coupling constants $\bar{g}_{\alpha\beta}$ can then be introduced through the relation

$$\int_{\text{u.c.}} d^2\mathbf{r}' g_{\alpha\beta} |\psi_{\alpha}(\mathbf{r}', t)|^2 |\psi_{\beta}(\mathbf{r}', t)|^2 = 2\pi\ell^2 \bar{g}_{\alpha\beta} n_{\alpha}(\mathbf{r}, t) n_{\beta}(\mathbf{r}, t), \quad (6)$$

where $|\psi_{\alpha}|^2$ and n_{α} are the original and coarse-grained densities of the spin- α atoms, respectively, and the integration on the left-hand side is taken over the unit cell (with the area $2\pi\ell^2$) that contains \mathbf{r} . As explained later in this section and in section 4.1, the renormalized constants $\bar{g}_{\alpha\beta}$ for describing the low-energy physics can be determined by calculating the contribution of each interaction term to the mean-field ground-state energy. As seen in equation (6), a positive (negative) correlation between the density fluctuations $|\psi_{\alpha}|^2 - n_{\alpha}$ and $|\psi_{\beta}|^2 - n_{\beta}$ leads to an enhanced (reduced) renormalized coupling $|\bar{g}_{\alpha\beta}| > |g_{\alpha\beta}|$ ($|\bar{g}_{\alpha\beta}| < |g_{\alpha\beta}|$). In particular, the intracomponent coupling g is always enhanced by the renormalization while the intercomponent repulsion $g_{\uparrow\downarrow} > 0$ (attraction $g_{\uparrow\downarrow} < 0$) is reduced (enhanced) by the renormalization owing to the separation (overlap) of vortices between the two components; this can be confirmed in figure 2 below. For a rotating scalar BEC with a repulsive coupling $g > 0$, a similar renormalization with $\bar{g}/g = 1.1596$ has been discussed in references [7, 18, 66]. At high filling factors $\nu \gg 1$ and for not too large a number of vortices N_v , we can assume that the condensates are only weakly depleted; we therefore have $|n_{\alpha}(\mathbf{r}, t) - n| \ll n$ for the coarse-grained density n_{α} .

Because the displacement fields $\{\mathbf{u}_{\alpha}\}$ involve the mass term $-\mathbf{u}_{\alpha}^2$ in equation (5), one may safely integrate them out in the discussion of low-energy dynamics. Instead of performing the integration directly, it is useful to derive the Euler–Lagrange equations for $\{\mathbf{u}_{\alpha}\}$:

$$\begin{aligned} \mathbf{u}_{\alpha} - \epsilon_{\alpha} \ell^2 \mathbf{e}_z \times \nabla \theta_{\alpha} - \frac{\epsilon_{\alpha}}{\omega_c} \mathbf{e}_z \times \dot{\mathbf{u}}_{\alpha} \\ + \frac{\ell^2}{n\hbar\omega_c} \left[\frac{\partial \mathcal{E}_{\text{el}}}{\partial \mathbf{u}_{\alpha}} - \partial_j \left(\frac{\partial \mathcal{E}_{\text{el}}}{\partial (\partial_j \mathbf{u}_{\alpha})} \right) \right] = 0, \end{aligned} \quad (7)$$

where we have made the approximation $n_{\alpha} \approx n$. We can ignore the third and fourth terms on the left-hand side in the LLL approximation with $\hbar\omega, \mathcal{E}_{\text{el}}/n \ll \hbar\omega_c$, where ω is the frequency of our concern. Introducing $\mathbf{u}_{\pm} := \mathbf{u}_{\uparrow} \pm \mathbf{u}_{\downarrow}$ and $\theta_{\pm} := \theta_{\uparrow} \pm \theta_{\downarrow}$, we can rewrite equation (7) as

$$\mathbf{u}_{\pm} = \begin{cases} \ell^2 \mathbf{e}_z \times \nabla \theta_{\pm} & \text{(parallel fields);} \\ \ell^2 \mathbf{e}_z \times \nabla \theta_{\mp} & \text{(antiparallel fields).} \end{cases} \quad (8)$$

These relations indicate that the (anti)symmetric movement of vortices is coupled to the (anti)symmetric component of the phase variables for parallel fields, while they are coupled in a crossed manner for antiparallel fields. By substituting equation (8) into equation (5), we obtain the effective Lagrangian in terms of θ_{\pm} and their conjugate momenta $\hbar n_{\pm} = \hbar(n_{\uparrow} \pm n_{\downarrow})/2$. The Hamiltonian density is then obtained as

$$\mathcal{H} = \sum_{\nu=\pm} \left[\bar{g}_{\nu} n_{\nu}^2 + \frac{\hbar^2 (\nabla n_{\nu})^2}{4nM} \right] + \mathcal{E}_{\text{el}}, \quad \bar{g}_{\pm} := \bar{g} \pm \bar{g}_{\uparrow\downarrow}, \quad (9)$$

where \mathcal{E}_{el} is expressed in terms of the phase variables θ_{\pm} by using equation (8). The theory can be quantized by requiring the canonical commutation relations

$$[\theta_{\nu}(\mathbf{r}), n_{\nu'}(\mathbf{r}')] = i\delta_{\nu\nu'}\delta(\mathbf{r} - \mathbf{r}') \quad (\nu, \nu' = \pm). \quad (10)$$

In the present coarse-grained description, the mean-field ground state corresponds to the uniform state with $n_{+}(\mathbf{r}) = n$, $n_{-}(\mathbf{r}) = 0$, and $\nabla\theta_{\pm}(\mathbf{r}) = 0$. Therefore, using equation (9), we obtain the mean-field ground-state energy density as

$$\frac{E_{\text{GS}}^{\text{MF}}}{A} = \bar{g}_{+} n^2 = (\bar{g} + \bar{g}_{\uparrow\downarrow}) n^2 = \frac{1}{2} \sum_{\alpha, \beta} \bar{g}_{\alpha\beta} n^2. \quad (11)$$

In contrast, the same energy density obtained by the microscopic calculation (the first term of equation (67) shown later) has the form $E_{\text{GS}}^{\text{MF}}/A = (\beta g + \beta_{\uparrow\downarrow} g_{\uparrow\downarrow}) n^2$, where β and $\beta_{\uparrow\downarrow}$ are dimensionless constants that depend on the lattice structure. The renormalized coupling constants are thus determined as $\bar{g} = \beta g$ and $\bar{g}_{\uparrow\downarrow} = \beta_{\uparrow\downarrow} g_{\uparrow\downarrow}$.

2.3. Elastic energy

The expression of the elastic energy density \mathcal{E}_{el} has been determined in references [45, 46], and we summarize it in the following. We first note that the elastic energy must be invariant under a constant change in $\mathbf{u}_{\alpha}(\mathbf{r}, t)$, i.e., translation of the lattices. Therefore, to the leading order in the derivative

expansion, \mathcal{E}_{el} should be a function of $\partial_i \mathbf{u}_+$ ($i = x, y$) and \mathbf{u}_- , resulting in the decomposition

$$\mathcal{E}_{\text{el}} = \mathcal{E}_{\text{el}}^{(+)}(\partial_i \mathbf{u}_+) + \mathcal{E}_{\text{el}}^{(-)}(\mathbf{u}_-) + \mathcal{E}_{\text{el}}^{(+-)}(\partial_i \mathbf{u}_+, \mathbf{u}_-). \quad (12)$$

To express $\mathcal{E}_{\text{el}}^{(+)}$, it is useful to introduce

$$w_1 := \partial_x u_+^x - \partial_y u_+^y, \quad w_2 := \partial_y u_+^x + \partial_x u_+^y. \quad (13)$$

On the basis of a symmetry consideration, each term in equation (12) can be expressed as

$$\mathcal{E}_{\text{el}}^{(+)}(\partial_i \mathbf{u}_+) = \frac{gn^2}{2} (C_1 w_1^2 + C_2 w_2^2 + C_3 w_1 w_2), \quad (14a)$$

$$\mathcal{E}_{\text{el}}^{(-)}(\mathbf{u}_-) = \frac{gn^2}{2\ell^2} \left[D_1 (u_-^x)^2 + D_2 (u_-^y)^2 + D_3 u_-^x u_-^y \right], \quad (14b)$$

$$\mathcal{E}_{\text{el}}^{(+-)}(\partial_i \mathbf{u}_+, \mathbf{u}_-) = \frac{gn^2}{2\ell} F_1 (w_1 u_-^y + w_2 u_-^x). \quad (14c)$$

For each of the vortex-lattice structures in figures 1(a)–(e), the dimensionless elastic constants $\{C_1, C_2, C_3, D_1, D_2, D_3, F_1\}$ satisfy

- (a) $C_1 = C_2 \equiv C > 0, \quad D_1 = D_2 \equiv D > 0, \quad C_3 = D_3 = F_1 = 0;$
- (b) $C_1 = C_2 \equiv C > 0, \quad D_1 = D_2 \equiv D > 0, \quad C_3 = D_3 = 0, \quad F_1 \neq 0;$
- (c) $C_1, C_2, D_1, D_2 > 0, \quad C_3, D_3 \neq 0, \quad F_1 = 0;$
- (d) $C_1, C_2 > 0, \quad D_1 = D_2 \equiv D > 0, \quad C_3 = D_3 = F_1 = 0;$
- (e) $C_1, C_2 > 0, \quad D_1, D_2 > 0, \quad C_3 = D_3 = F_1 = 0.$

(15)

Keçeli and Oktel [45] have determined the constants $\{C_1, C_2, C_3, D_1, D_2, D_3\}$ by calculating a change in the mean-field energy under deformation of vortex lattices. In our previous work [46], we have pointed out the presence of the F_1 term for interlaced triangular vortex lattices (b), which was missed in reference [45]. For $\nu \gg 1$, the elastic constants should be the same for the two types of fields because of the exact correspondence of the GP energy functionals [42]. In section 4.2, we will determine all the elastic constants above as a function of $g_{\uparrow\downarrow}/g$ by using the data of the excitation spectra.

2.4. Diagonalization of the effective Hamiltonian

We are now in a position to calculate the energy spectrum of the Hamiltonian $H = \int d^2 \mathbf{r} \mathcal{H}$, where the Hamiltonian density \mathcal{H} is given by equation (9). We perform Fourier expansions

$$\theta_\nu(\mathbf{r}) = \frac{1}{\sqrt{A}} \sum_{\mathbf{k}} \theta_{\mathbf{k},\nu} e^{i\mathbf{k}\cdot\mathbf{r}}, \quad (16a)$$

$$n_\nu(\mathbf{r}) = \frac{1}{\sqrt{A}} \sum_{\mathbf{k}} n_{\mathbf{k},\nu} e^{i\mathbf{k}\cdot\mathbf{r}} \quad (\nu = \pm), \quad (16b)$$

where the Fourier components satisfy

$$[\theta_{\mathbf{k},\nu}, n_{-\mathbf{k}',\nu'}] = i\delta_{\nu\nu'}\delta_{\mathbf{k}\mathbf{k}'}, \quad (17a)$$

$$\theta_{\mathbf{k},\nu}^\dagger = \theta_{-\mathbf{k},\nu}, \quad n_{\mathbf{k},\nu}^\dagger = n_{-\mathbf{k},\nu} \quad (\nu, \nu' = \pm). \quad (17b)$$

We note that the $\mathbf{k} = \mathbf{0}$ component $n_{\mathbf{0},\pm}$ of the densities is related to the atom numbers as $n_{\mathbf{0},\pm} = (N_\uparrow \pm N_\downarrow)/(2\sqrt{A})$. The Hamiltonian H is then expressed as

$$H = \frac{n}{2} \sum_{\mathbf{k}} \begin{pmatrix} \theta_{-\mathbf{k},+} & \theta_{-\mathbf{k},-} \end{pmatrix} \begin{pmatrix} \Gamma_\pm(\mathbf{k}) & \pm i\Gamma(\mathbf{k}) \\ \mp i\Gamma(\mathbf{k}) & \Gamma_\mp(\mathbf{k}) \end{pmatrix} \begin{pmatrix} \theta_{\mathbf{k},+} \\ \theta_{\mathbf{k},-} \end{pmatrix} + \frac{1}{2n} \sum_{\mathbf{k}} \sum_{\nu=\pm} e_{\mathbf{k},\nu} n_{-\mathbf{k},\nu} n_{\mathbf{k},\nu}, \quad (18)$$

where⁶

$$e_{\mathbf{k},\nu} := 2\bar{g}_\nu n + \frac{\hbar^2 \mathbf{k}^2}{2M}, \quad (19a)$$

$$\Gamma_+(\mathbf{k}) := gn\ell^4 \left[C_1 (2k_x k_y)^2 + C_2 (k_x^2 - k_y^2)^2 - C_3 (2k_x k_y) (k_x^2 - k_y^2) \right], \quad (19b)$$

$$\Gamma_-(\mathbf{k}) := gn\ell^2 (D_1 k_y^2 + D_2 k_x^2 - D_3 k_x k_y), \quad (19c)$$

$$\Gamma(\mathbf{k}) := \frac{1}{2} gn\ell^3 F_1 [(2k_x k_y) k_x + (k_x^2 - k_y^2) k_y]. \quad (19d)$$

In equation (18), the upper and lower signs correspond to the cases of parallel and antiparallel fields, respectively.⁷

It is useful to decompose the Hamiltonian (18) into the zero-mode ($\mathbf{k} = \mathbf{0}$) and oscillator-mode ($\mathbf{k} \neq \mathbf{0}$) parts. First, the zero-mode part is given by

$$H^{\text{zero}} = \sum_{\nu=\pm} \bar{g}_\nu n_{\mathbf{0},\nu}^2 = \frac{\bar{g}_+}{4A} N^2 + \frac{\bar{g}_-}{4A} (N_\uparrow - N_\downarrow)^2. \quad (20)$$

Thus, the zero-mode energy is specified by the atom numbers N_\uparrow and N_\downarrow . In our setting of balanced population $N_\uparrow = N_\downarrow$, the zero-mode state is given by the product state $|N_\uparrow = N/2\rangle |N_\downarrow = N/2\rangle$, which has no intercomponent entanglement.

Next, we discuss the oscillator-mode part H^{osc} of the Hamiltonian (18). To treat this part, we perform canonical transformations in two steps. The first transformation reads

$$\tilde{\theta}_{\mathbf{k},+} = r_{\mathbf{k}}^{-1} \theta_{\mathbf{k},+}, \quad \tilde{\theta}_{\mathbf{k},-} = r_{\mathbf{k}} \theta_{\mathbf{k},-}, \quad (21a)$$

$$\tilde{n}_{\mathbf{k},+} = r_{\mathbf{k}} n_{\mathbf{k},+}, \quad \tilde{n}_{\mathbf{k},-} = r_{\mathbf{k}}^{-1} n_{\mathbf{k},-}, \quad (21b)$$

where $r_{\mathbf{k}} := (e_{\mathbf{k},+}/e_{\mathbf{k},-})^{1/4}$. Then, H^{osc} is rewritten as

$$H^{\text{osc}} = \frac{n}{2} \sum_{\mathbf{k} \neq \mathbf{0}} \begin{pmatrix} \tilde{\theta}_{-\mathbf{k},+} & \tilde{\theta}_{-\mathbf{k},-} \end{pmatrix} M(\mathbf{k}) \begin{pmatrix} \tilde{\theta}_{\mathbf{k},+} \\ \tilde{\theta}_{\mathbf{k},-} \end{pmatrix} + \frac{1}{2n} \sum_{\mathbf{k} \neq \mathbf{0}} \sum_{\nu=\pm} e_{\mathbf{k},\nu} \tilde{n}_{-\mathbf{k},\nu} \tilde{n}_{\mathbf{k},\nu}, \quad (22)$$

⁶ We slightly change the definitions of $\Gamma_\pm(\mathbf{k})$ and $\Gamma(\mathbf{k})$ from reference [46] by dividing them by n so that they have the dimension of energy.

⁷ The same sign rule applies to equations (23), (24), (27), (32), (34), (35), (43), (44), (51), (56), (A.5) and (A.6) below.

where $e_{\mathbf{k}} := \sqrt{e_{\mathbf{k},+} e_{\mathbf{k},-}}$. Here, the 2×2 matrix $M(\mathbf{k})$ is given by

$$M(\mathbf{k}) := \begin{pmatrix} r_{\mathbf{k}}^2 \Gamma_{\pm}(\mathbf{k}) & \pm i \Gamma(\mathbf{k}) \\ \mp i \Gamma(\mathbf{k}) & r_{\mathbf{k}}^{-2} \Gamma_{\mp}(\mathbf{k}) \end{pmatrix} \quad (23)$$

$$= \Gamma_0(\mathbf{k}) I \mp \Gamma(\mathbf{k}) \sigma_y + \Gamma_z(\mathbf{k}) \sigma_z,$$

where I is the identity matrix, $(\sigma_x, \sigma_y, \sigma_z)$ are the Pauli matrices, and

$$\Gamma_0(\mathbf{k}) := \frac{1}{2} [r_{\mathbf{k}}^2 \Gamma_{\pm}(\mathbf{k}) + r_{\mathbf{k}}^{-2} \Gamma_{\mp}(\mathbf{k})], \quad (24a)$$

$$\Gamma_z(\mathbf{k}) := \frac{1}{2} [r_{\mathbf{k}}^2 \Gamma_{\pm}(\mathbf{k}) - r_{\mathbf{k}}^{-2} \Gamma_{\mp}(\mathbf{k})]. \quad (24b)$$

We then perform the second canonical transformation using the unitary matrix $U(\mathbf{k})$ as

$$\begin{pmatrix} \tilde{\theta}_{\mathbf{k},+} \\ \tilde{\theta}_{\mathbf{k},-} \end{pmatrix} = U(\mathbf{k}) \begin{pmatrix} \bar{\theta}_{\mathbf{k},1} \\ \bar{\theta}_{\mathbf{k},2} \end{pmatrix}, \quad \begin{pmatrix} \tilde{n}_{\mathbf{k},+} \\ \tilde{n}_{\mathbf{k},-} \end{pmatrix} = U(\mathbf{k}) \begin{pmatrix} \bar{n}_{\mathbf{k},1} \\ \bar{n}_{\mathbf{k},2} \end{pmatrix}. \quad (25)$$

We note that the second term of equation (22) is invariant under this transformation if $U(-\mathbf{k})^T U(\mathbf{k}) = I$ for all $\mathbf{k} \neq \mathbf{0}$. It is therefore useful to choose $U(\mathbf{k})$ in such a way as to diagonalize the Hermitian matrix $M(\mathbf{k})$ as

$$U^{-1}(\mathbf{k}) M(\mathbf{k}) U(\mathbf{k}) = \begin{pmatrix} m_{\mathbf{k},1} & 0 \\ 0 & m_{\mathbf{k},2} \end{pmatrix}, \quad (26a)$$

$$U(\mathbf{k}) = e^{i \chi_{\mathbf{k}} \sigma_x / 2} = \begin{pmatrix} \cos(\chi_{\mathbf{k}}/2) & i \sin(\chi_{\mathbf{k}}/2) \\ i \sin(\chi_{\mathbf{k}}/2) & \cos(\chi_{\mathbf{k}}/2) \end{pmatrix}, \quad (26b)$$

where⁸

$$m_{\mathbf{k},j} := \Gamma_0(\mathbf{k}) + (-1)^{j-1} \Lambda(\mathbf{k}) \quad (j = 1, 2), \quad (27a)$$

$$\Lambda(\mathbf{k}) (\cos \chi_{\mathbf{k}}, \sin \chi_{\mathbf{k}}) := (\Gamma_z(\mathbf{k}), \Gamma(\mathbf{k})). \quad (27b)$$

In terms of the new set of canonical variables, the Hamiltonian (22) is further rewritten as

$$H^{\text{osc}} = \frac{1}{2} \sum_{\mathbf{k} \neq \mathbf{0}} \sum_{j=1,2} \left(n m_{\mathbf{k},j} \bar{\theta}_{-\mathbf{k},j} \bar{\theta}_{\mathbf{k},j} + \frac{e_{\mathbf{k}}}{n} \bar{n}_{-\mathbf{k},j} \bar{n}_{\mathbf{k},j} \right). \quad (28)$$

Here, $\bar{\theta}_{\mathbf{k},j}$ and $\bar{n}_{\mathbf{k},j}$ satisfy $[\bar{\theta}_{\mathbf{k},j}, \bar{n}_{-\mathbf{k}',j'}] = i \delta_{jj'} \delta_{\mathbf{k}\mathbf{k}'} (\mathbf{k}, \mathbf{k}' \neq \mathbf{0}; j, j' = 1, 2)$ as the transformations in equations (21) and (25) leave the commutation relations unchanged. Finally, introducing the (bogolon) annihilation and creation operators

$$\gamma_{\mathbf{k},j} := \frac{1}{\sqrt{2}} \left(\sqrt{n} \zeta_{\mathbf{k},j} \bar{\theta}_{\mathbf{k},j} + \frac{i \bar{n}_{\mathbf{k},j}}{\sqrt{n} \zeta_{\mathbf{k},j}} \right), \quad (29a)$$

$$\gamma_{\mathbf{k},j}^{\dagger} := \frac{1}{\sqrt{2}} \left(\sqrt{n} \zeta_{\mathbf{k},j} \bar{\theta}_{\mathbf{k},j} - \frac{i \bar{n}_{\mathbf{k},j}}{\sqrt{n} \zeta_{\mathbf{k},j}} \right) \quad (\mathbf{k} \neq \mathbf{0}; j = 1, 2), \quad (29b)$$

⁸ Since $\Gamma_z(\mathbf{k}) = \Gamma_z(-\mathbf{k})$ and $\Gamma(-\mathbf{k}) = -\Gamma(\mathbf{k})$, we find $\chi_{-\mathbf{k}} = -\chi_{\mathbf{k}}$ and thus $U(-\mathbf{k})^T = U(\mathbf{k})^{\dagger} = U(\mathbf{k})^{-1}$; therefore, the aforementioned condition $U(-\mathbf{k})^T U(\mathbf{k}) = I$ is met.

with $\zeta_{\mathbf{k},j} := (m_{\mathbf{k},j} / e_{\mathbf{k}})^{1/4}$, we can diagonalize the Hamiltonian (28) as

$$H^{\text{osc}} = \sum_{\mathbf{k} \neq \mathbf{0}} \sum_{j=1,2} E_j(\mathbf{k}) \left(\gamma_{\mathbf{k},j}^{\dagger} \gamma_{\mathbf{k},j} + \frac{1}{2} \right), \quad (30a)$$

$$E_j(\mathbf{k}) := \sqrt{m_{\mathbf{k},j} e_{\mathbf{k}}}. \quad (30b)$$

The ground state $|0^{\text{osc}}\rangle$ of this Hamiltonian is specified by the condition that $\gamma_{\mathbf{k},\pm} |0^{\text{osc}}\rangle = 0$ for all $\mathbf{k} \neq \mathbf{0}$.

We now discuss the single-particle spectrum $E_j(\mathbf{k})$ ($j = 1, 2$) in the long-wavelength limit $k\ell \ll 1$. In this limit, we can make the approximation $r_{\mathbf{k}} \approx r_{\mathbf{0}} = (\bar{g}_+ / \bar{g}_-)^{1/4}$ and $e_{\mathbf{k}} \approx e_{\mathbf{0}} = 2(\bar{g}_+ \bar{g}_-)^{1/2} n$. Since $\Gamma_+(\mathbf{k}) = \mathcal{O}(k^4)$, $\Gamma_-(\mathbf{k}) = \mathcal{O}(k^2)$, and $\Gamma(\mathbf{k}) = \mathcal{O}(k^3)$ as seen in equation (19), we can approximate $m_{\mathbf{k},j}$ in equation (27) as

$$m_{\mathbf{k},1} \approx r_{\mathbf{0}}^{\mp 2} \Gamma_-(\mathbf{k}), \quad m_{\mathbf{k},2} \approx r_{\mathbf{0}}^{\pm 2} \left[\Gamma_+(\mathbf{k}) - \frac{\Gamma(\mathbf{k})^2}{\Gamma_-(\mathbf{k})} \right]. \quad (31)$$

By parametrizing the wave vector as $(k_x, k_y) = k(\cos \varphi, \sin \varphi)$, $m_{\mathbf{k},j}$ can also be expressed as

$$m_{\mathbf{k},1} \approx r_{\mathbf{0}}^{\mp 2} g n D(\varphi) (k\ell)^2, \quad m_{\mathbf{k},2} \approx r_{\mathbf{0}}^{\pm 2} g n C(\varphi) (k\ell)^4, \quad (32)$$

where

$$C(\varphi) := C_1 \sin^2(2\varphi) + C_2 \cos^2(2\varphi) - C_3 \sin(2\varphi) \cos(2\varphi) - C_4 \sin^2(3\varphi), \quad (33a)$$

$$D(\varphi) := D_1 \sin^2(\varphi) + D_2 \cos^2(\varphi) - D_3 \sin(\varphi) \cos(\varphi), \quad (33b)$$

with $C_4 := F_1^2 / 4D_1$. We then obtain the low-energy spectrum as

$$E_j(\mathbf{k}) \approx \sqrt{m_{\mathbf{k},j} e_{\mathbf{0}}} \approx \sqrt{2} g n (k\ell)^j f_j(\varphi) \quad (j = 1, 2), \quad (34)$$

where the dependence on the angle φ is expressed by the dimensionless functions

$$f_1(\varphi) = \sqrt{\bar{g}_{\mp} D(\varphi) / g}, \quad f_2(\varphi) = \sqrt{\bar{g}_{\pm} C(\varphi) / g}. \quad (35)$$

We thus find that low-energy modes with linear and quadratic dispersion relations emerge with anisotropy that depends on the lattice structure. Furthermore, the low-energy dispersion relations for parallel (P) and antiparallel (AP) fields are related by proper rescaling as follows:

$$E_1^{\text{P}}(\mathbf{k}) / \sqrt{\bar{g}_-} = E_1^{\text{AP}}(\mathbf{k}) / \sqrt{\bar{g}_+}, \quad (36a)$$

$$E_2^{\text{P}}(\mathbf{k}) / \sqrt{\bar{g}_+} = E_2^{\text{AP}}(\mathbf{k}) / \sqrt{\bar{g}_-}. \quad (36b)$$

Using the dimensionless functions $f_j(\varphi)$ ($j = 1, 2$) for the two types of fields, these relations can also be written as

$$f_1^{\text{P}}(\varphi) \sqrt{\frac{g}{\bar{g}_-}} = f_1^{\text{AP}}(\varphi) \sqrt{\frac{g}{\bar{g}_+}} = \sqrt{D(\varphi)}, \quad (37a)$$

$$f_2^{\text{P}}(\varphi) \sqrt{\frac{g}{\bar{g}_+}} = f_2^{\text{AP}}(\varphi) \sqrt{\frac{g}{\bar{g}_-}} = \sqrt{C(\varphi)}. \quad (37b)$$

In section 4.2, we will confirm these relations through the numerical calculations by the Bogoliubov theory for all the five vortex-lattice structures in figures 1(a)–(e). While similar rescaling relations are also discussed in reference [46], the importance of using the renormalized coupling constants \bar{g}_\pm is overlooked there. Without the renormalization, the rescaling relations in equations (36) and (37) are satisfied only for overlapping vortex lattices where $\beta = \beta_{\uparrow\downarrow}$, as confirmed numerically in reference [46].

2.5. Intercomponent entanglement

We now calculate the reduced density matrix (RDM) ρ_\uparrow for the spin- \uparrow component, which is defined by starting from the ground state $|0^{\text{zero}}\rangle \otimes |0^{\text{osc}}\rangle$ of the total system and trancing out the degrees of freedom in the spin- \downarrow component. We then discuss the properties of the intercomponent entanglement. Because of the decoupling of the zero and oscillator modes, the RDM takes the form of $\rho_\uparrow = \rho_\uparrow^{\text{zero}} \otimes \rho_\uparrow^{\text{osc}}$. As the zero-mode ground state $|N_\uparrow = N/2\rangle |N_\downarrow = N/2\rangle$ is a product state, there is no intercomponent entanglement in the zero-mode part; the RDM in this part is given simply by $\rho_\uparrow^{\text{zero}} = |N_\uparrow = N/2\rangle \langle N_\uparrow = N/2|$. Below we consider the oscillator-mode part $\rho_\uparrow^{\text{osc}}$.

For $\rho_\uparrow^{\text{osc}}$, we introduce the following Gaussian ansatz [61–63, 67–69]:

$$\rho_\uparrow^{\text{osc}} = \frac{1}{Z_e^{\text{osc}}} e^{-H_e^{\text{osc}}}, \quad Z_e^{\text{osc}} = \text{Tr } e^{-H_e^{\text{osc}}}, \quad (38\text{a})$$

$$H_e^{\text{osc}} = \frac{1}{2} \sum_{\mathbf{k} \neq \mathbf{0}} \left(n F_{\mathbf{k}} \theta_{-\mathbf{k},\uparrow} \theta_{\mathbf{k},\uparrow} + \frac{G_{\mathbf{k}}}{n} n_{-\mathbf{k},\uparrow} n_{\mathbf{k},\uparrow} \right), \quad (38\text{b})$$

where $F_{\mathbf{k}}$ and $G_{\mathbf{k}}$ are positive dimensionless coefficients to be determined later and we assume $F_{\mathbf{k}} = F_{-\mathbf{k}}$ and $G_{\mathbf{k}} = G_{-\mathbf{k}}$ for convenience. By introducing annihilation and creation operators as

$$\eta_{\mathbf{k}} = \frac{1}{\sqrt{2}} \left[\sqrt{n} \left(\frac{F_{\mathbf{k}}}{G_{\mathbf{k}}} \right)^{1/4} \theta_{\mathbf{k},\uparrow} + \frac{i}{\sqrt{n}} \left(\frac{G_{\mathbf{k}}}{F_{\mathbf{k}}} \right)^{1/4} n_{\mathbf{k},\uparrow} \right], \quad (39\text{a})$$

$$\eta_{\mathbf{k}}^\dagger = \frac{1}{\sqrt{2}} \left[\sqrt{n} \left(\frac{F_{\mathbf{k}}}{G_{\mathbf{k}}} \right)^{1/4} \theta_{-\mathbf{k},\uparrow} - \frac{i}{\sqrt{n}} \left(\frac{G_{\mathbf{k}}}{F_{\mathbf{k}}} \right)^{1/4} n_{-\mathbf{k},\uparrow} \right] \quad (\mathbf{k} \neq \mathbf{0}), \quad (39\text{b})$$

the entanglement Hamiltonian H_e^{osc} in equation (38) is diagonalized as

$$H_e^{\text{osc}} = \sum_{\mathbf{k} \neq \mathbf{0}} \xi_{\mathbf{k}} \left(\eta_{\mathbf{k}}^\dagger \eta_{\mathbf{k}} + \frac{1}{2} \right), \quad (40)$$

where $\xi_{\mathbf{k}} := \sqrt{F_{\mathbf{k}} G_{\mathbf{k}}}$ is the single-particle ES.

The single-particle ES $\xi_{\mathbf{k}}$ and the coefficients $F_{\mathbf{k}}$ and $G_{\mathbf{k}}$ can be determined in the following way [61]. Using the relations

in equation (39) and the Bose distribution function

$$\text{Tr} \left(\eta_{\mathbf{k}}^\dagger \eta_{\mathbf{k}} \rho_\uparrow^{\text{osc}} \right) = \frac{1}{e^{\xi_{\mathbf{k}} - 1}} \equiv f_B(\xi_{\mathbf{k}}), \quad (41)$$

we obtain the phase and density correlators as

$$\text{Tr} \left(\theta_{-\mathbf{k},\uparrow} \theta_{\mathbf{k},\uparrow} \rho_\uparrow^{\text{osc}} \right) = \frac{1}{n} \left(\frac{G_{\mathbf{k}}}{F_{\mathbf{k}}} \right)^{1/2} \left[f_B(\xi_{\mathbf{k}}) + \frac{1}{2} \right], \quad (42\text{a})$$

$$\text{Tr} \left(n_{-\mathbf{k},\uparrow} n_{\mathbf{k},\uparrow} \rho_\uparrow^{\text{osc}} \right) = n \left(\frac{F_{\mathbf{k}}}{G_{\mathbf{k}}} \right)^{1/2} \left[f_B(\xi_{\mathbf{k}}) + \frac{1}{2} \right]. \quad (42\text{b})$$

We can then determine $f_B(\xi_{\mathbf{k}})$ and $F_{\mathbf{k}}/G_{\mathbf{k}}$ by requiring these correlators to be equal to the same correlators calculated for the oscillator ground state $|0^{\text{osc}}\rangle$ of the total system. Details of this calculation are described in appendix A. In the long-wavelength limit $k\ell \ll 1$, we obtain

$$\xi_{\mathbf{k}} \approx c(\varphi) \sqrt{k\ell}, \quad F_{\mathbf{k}} \approx F(\varphi)(k\ell)^2, \quad G_{\mathbf{k}} \approx \frac{G(\varphi)}{k\ell}, \quad (43)$$

where the dependences on the angle φ are expressed by the dimensionless functions

$$c(\varphi) = 4 \left[\frac{\bar{g}_\pm C(\varphi)}{\bar{g}_\pm D(\varphi)} \right]^{1/4}, \quad (44\text{a})$$

$$F(\varphi) = 4 \sqrt{\frac{2gC(\varphi)}{\bar{g}_\pm}}, \quad G(\varphi) = 2 \sqrt{\frac{2\bar{g}_\mp}{gD(\varphi)}}. \quad (44\text{b})$$

We find that the ES shows a gapless square-root dispersion relation with anisotropy that depends on the lattice structure. Furthermore, similarly to the case of excitation spectra (see equation (36)), the single-particle ES $\xi_{\mathbf{k}}^P$ for parallel (P) fields and that $\xi_{\mathbf{k}}^{\text{AP}}$ for antiparallel (AP) fields are related by suitable rescaling as

$$\left(\frac{\bar{g}_+}{\bar{g}_-} \right)^{1/4} \xi_{\mathbf{k}}^P = \left(\frac{\bar{g}_-}{\bar{g}_+} \right)^{1/4} \xi_{\mathbf{k}}^{\text{AP}}. \quad (45)$$

Using the dimensionless functions $c(\varphi)$ for the two types of fields, this relation can also be written as

$$\left(\frac{\bar{g}_+}{\bar{g}_-} \right)^{1/4} c^P(\varphi) = \left(\frac{\bar{g}_-}{\bar{g}_+} \right)^{1/4} c^{\text{AP}}(\varphi) = 4 \left[\frac{C(\varphi)}{D(\varphi)} \right]^{1/4}. \quad (46)$$

The entanglement Hamiltonian is given in the long-wavelength limit by H_e^{osc} in equation (38) with $F_{\mathbf{k}}$ and $G_{\mathbf{k}}$ in equation (43). Using the fields $\theta_\uparrow(\mathbf{r})$ and $n_\uparrow(\mathbf{r})$ in real space, it can be expressed as

$$H_e = \int d^2\mathbf{r} \int d^2\mathbf{r}' \left[\frac{n\ell^2}{2} U_F(\mathbf{r} - \mathbf{r}') \nabla \theta_\uparrow(\mathbf{r}) \cdot \nabla \theta_\uparrow(\mathbf{r}') + \frac{1}{2n} U_G(\mathbf{r} - \mathbf{r}') n_\uparrow(\mathbf{r}) n_\uparrow(\mathbf{r}') \right], \quad (47)$$

where we introduce the interaction potentials

$$U_F(\mathbf{r} - \mathbf{r}') = \frac{1}{A} \sum_{\mathbf{k}} F(\varphi) e^{i\mathbf{k} \cdot (\mathbf{r} - \mathbf{r}')}, \quad (48a)$$

$$U_G(\mathbf{r} - \mathbf{r}') = \lim_{\alpha \rightarrow 0^+} \frac{1}{A} \sum_{\mathbf{k} \neq \mathbf{0}} \frac{G(\varphi)}{k\ell} e^{-\alpha k + i\mathbf{k} \cdot (\mathbf{r} - \mathbf{r}')}. \quad (48b)$$

Here, we use the convergence factor $e^{-\alpha k}$ to regularize the infinite sum for $U_G(\mathbf{r} - \mathbf{r}')$. For simplicity, we consider the case of overlapping triangular lattices, in which $C(\varphi)$ and $D(\varphi)$ (and thus $F(\varphi)$ and $G(\varphi)$ as well) are constant; see (a) in equation (15). In this case, the potentials in equation (48) are calculated as

$$U_F(\mathbf{r} - \mathbf{r}') = F\delta(\mathbf{r} - \mathbf{r}'), \quad (49a)$$

$$U_G(\mathbf{r} - \mathbf{r}') = \frac{G}{2\pi\ell|\mathbf{r} - \mathbf{r}'|}. \quad (49b)$$

For the calculation of $U_G(\mathbf{r} - \mathbf{r}')$, we refer the reader to appendix A of reference [61]. We note that $\theta_{\uparrow}(\mathbf{r})$ is the regular part of the superfluid phase of the spin- \uparrow component, and that its gradient is related to the regular part of the superfluid velocity, $\mathbf{v}_{s,\uparrow}(\mathbf{r}) = -\frac{\hbar}{M} \nabla \theta_{\uparrow}(\mathbf{r})$. Therefore, the entanglement Hamiltonian (47) has a short-range interaction in terms of the superfluid velocity $\mathbf{v}_{s,\uparrow}(\mathbf{r})$ and a long-range one in terms of the density $n_{\uparrow}(\mathbf{r})$. If the density-density interaction were short-ranged, the ES would show a phonon mode with a linear dispersion relation. Therefore, the anomalous square-root dispersion relation in equation (43) is closely related with the presence of a long-range interaction in H_e .

Using the single-particle ES $\xi_{\mathbf{k}}$ in equation (43), we can calculate the intercomponent EE S_e . For simplicity, we assume that $\xi_{\mathbf{k}}$ is isotropic, i.e., $c(\varphi)$ is constant, as in the case of overlapping triangular lattices; however, we expect that the result holds qualitatively for all the lattice structures. With this simplification, the EE is calculated as (see appendix B of reference [61] for the derivation)

$$\begin{aligned} S_e &= \frac{\sigma A}{c^4 \ell^2} - \frac{1}{2} \ln \frac{\sqrt{A}}{2\pi c^2 \ell} + O(1) \\ &= \frac{2\pi\sigma N_v}{c^4} - \frac{1}{4} \ln \frac{N_v}{2\pi c^4} + O(1). \end{aligned} \quad (50)$$

Here, the leading contribution is given by the first term, which is proportional to the area A with a non-universal coefficient σ that depends, e.g., on the choice of the high-momentum cutoff. Besides, there is a subleading logarithmic term with the universal coefficient (equal to $-1/2$ when written as a function of the linear system size \sqrt{A}), which is determined through a careful examination of small- k contributions and therefore originates from the Nambu–Goldstone modes. The intercomponent EE per flux in the thermodynamic limit is calculated as

$$\lim_{N_v \rightarrow \infty} \frac{S_e}{N_v} = \frac{2\pi\sigma}{c^4} = \frac{\pi\sigma\bar{g}_{\pm}D}{128\bar{g}_{\mp}C}. \quad (51)$$

Because of the factor $\bar{g}_{\pm}/\bar{g}_{\mp}$ in equation (51), when the intercomponent interaction $g_{\uparrow\downarrow}$ is repulsive (attractive), the intercomponent EE is expected to be larger for the case of parallel (antiparallel) fields. We note that the above calculation of

the intercomponent EE S_e is simple yet approximate as it is based on the single-particle ES $\xi_{\mathbf{k}}$ for long wavelengths. In section 4.3, we will present numerical results on S_e based on the Bogoliubov theory, in which $\xi_{\mathbf{k}}$ over the full Brillouin zone is taken into account, and confirm the consistency with the field-theoretical predictions.

2.6. Intracomponent correlation functions

Here we calculate some intracomponent correlation functions, and discuss their connections with the (long-wavelength) entanglement Hamiltonian H_e obtained in the preceding section. Let $\langle \mathcal{O} \rangle$ denote the expectation value of an operator \mathcal{O} with respect to the ground state $|0^{\text{zero}}\rangle \otimes |0^{\text{osc}}\rangle$ of the total system. If \mathcal{O} acts only on the spin- \uparrow component, $\langle \mathcal{O} \rangle$ should be equal to $\text{Tr}(\mathcal{O} e^{-H_e}) / \text{Tr} e^{-H_e}$ as far as long-distance properties are concerned. Our purpose here is to investigate how the unusual long-range interactions in H_e manifest themselves in the correlation properties of the system.

Owing to the gapless ES $\xi_{\mathbf{k}}$, we can approximate the Bose distribution function (41) as $f_B(\xi_{\mathbf{k}}) \approx \xi_{\mathbf{k}}^{-1} = (F_{\mathbf{k}} G_{\mathbf{k}})^{-1/2}$ for sufficiently small k . Then, in the long-wavelength limit, equation (42) gives

$$\langle \theta_{-\mathbf{k},\uparrow} \theta_{\mathbf{k},\uparrow} \rangle \approx \frac{1}{n F_{\mathbf{k}}} \approx \frac{1}{n F(\varphi) k^2 \ell^2}, \quad (52a)$$

$$\langle n_{-\mathbf{k},\uparrow} n_{\mathbf{k},\uparrow} \rangle \approx \frac{n}{G_{\mathbf{k}}} \approx \frac{n k \ell}{G(\varphi)} \quad (\mathbf{k} \neq \mathbf{0}), \quad (52b)$$

where we use equation (43). Therefore, the phase and density fluctuations are directly related to the coefficients $F_{\mathbf{k}}$ and $G_{\mathbf{k}}$, respectively, in the entanglement Hamiltonian (38). Equation (52) indicates that in the long-wavelength limit $k \rightarrow 0$, the phase fluctuation diverges and the density fluctuation is suppressed. From the viewpoint of the entanglement Hamiltonian, suppression of the density fluctuation is a consequence of the long-range interaction in terms of the density. The enhanced phase fluctuation in the long-wavelength limit leads to a quasi-long-range order in the one-particle density matrix, as we explain in the following.

The one-particle density matrix plays a key role in the characterization of the Bose–Einstein condensation [70–72]. To analyze its behavior in our coarse-grained description, we introduce the modified bosonic field $\tilde{\psi}_{\uparrow} = e^{-i\theta_{\uparrow}} \sqrt{n_{\uparrow}}$. As $\theta_{\uparrow}(\mathbf{r})$ is the regular part of the superfluid phase and $n_{\uparrow}(\mathbf{r})$ is the coarse-grained density, $\tilde{\psi}(\mathbf{r})$ is expected to vary slowly over space. We consider the modified one-particle density matrix

$$\langle \tilde{\psi}_{\uparrow}(\mathbf{r})^{\dagger} \tilde{\psi}_{\uparrow}(\mathbf{0}) \rangle = \left\langle \sqrt{n_{\uparrow}(\mathbf{r})} e^{i(\theta_{\uparrow}(\mathbf{r}) - \theta_{\uparrow}(\mathbf{0}))} \sqrt{n_{\uparrow}(\mathbf{0})} \right\rangle, \quad (53)$$

which describes the slowly varying component of the ordinary one-particle density matrix. Its long-distance behavior is determined dominantly by the phase fluctuation as seen in the small- k behavior of equation (52). Here we again consider the case of overlapping triangular lattices where $F(\varphi)$ is constant. By using equation (52), the phase correlation function in real

space is obtained as (see appendix B for the derivation)

$$\begin{aligned} \left\langle [\theta_{\uparrow}(\mathbf{r}) - \theta_{\uparrow}(\mathbf{0})]^2 \right\rangle &= \frac{2}{A} \sum_{\mathbf{k} \neq \mathbf{0}} e^{-\alpha k} [1 - \cos(\mathbf{k} \cdot \mathbf{r})] \langle \theta_{-\mathbf{k},\uparrow} \theta_{\mathbf{k},\uparrow} \rangle \\ &\approx \frac{1}{\pi n F \ell^2} \ln \frac{r}{2\alpha} \quad (r \gg \alpha), \end{aligned} \quad (54)$$

where we introduce the same convergence factor $e^{-\alpha k}$ as before to regularize the infinite sum. The modified one-particle density matrix is then obtained as

$$\begin{aligned} \langle \tilde{\psi}_{\uparrow}(\mathbf{r})^{\dagger} \tilde{\psi}_{\uparrow}(\mathbf{0}) \rangle &\approx n \exp \left\{ -\frac{1}{2} \left\langle [\theta_{\uparrow}(\mathbf{r}) - \theta_{\uparrow}(\mathbf{0})]^2 \right\rangle \right\} \\ &\approx n \left(\frac{r}{2\alpha} \right)^{-\frac{1}{2\pi n F \ell^2}}. \end{aligned} \quad (55)$$

We thus have a quasi-long-range order in the one-particle density matrix.

For a finite system of area A , the particle density n_0 of the condensate can be evaluated from the one-particle density matrix (55) at the large separation $r = \sqrt{A}/2$. The density n' of the depletion is then given by $n' = n - n_0$. Assuming $n' \ll n$ as required for the Bogoliubov theory and the present effective theory, the fraction of depletion is estimated as

$$\begin{aligned} \frac{n'}{n} &\approx \frac{1}{2} \left\langle [\theta_{\uparrow}(\mathbf{r}) - \theta_{\uparrow}(\mathbf{0})]^2 \right\rangle \Big|_{r=\sqrt{A}/2} \\ &\approx \frac{1}{2\pi n F \ell^2} \ln \frac{\sqrt{A}}{4\alpha} = \frac{1}{2\nu} \left(\frac{\bar{g}_{\pm}}{2gC} \right)^{1/2} \ln \frac{\sqrt{A}}{4\alpha}. \end{aligned} \quad (56)$$

where we use equation (44) and $\nu = 2nA/N_v = 4\pi n \ell^2$. For fixed ν , the fraction of quantum depletion of the condensate increases logarithmically as a function of the number of vortices $N_v = A/(2\pi \ell^2)$. Furthermore, for an intercomponent repulsion (attraction), it is larger for the case of parallel (antiparallel) fields, indicating larger quantum fluctuations. This behavior is in accord with the larger intercomponent EE given in equation (51). We note that a quasi-long-range order in the one-particle density matrix and a logarithmic increase of the fraction of depletion as in equations (55) and (56) have also been discussed for a vortex lattice in a scalar BEC [18, 20–22].

3. Bogoliubov theory

The Bogoliubov theory with the LLL approximation has been formulated for a scalar BEC in references [18, 21, 22]. In reference [46], we have applied this theory to the present problem of binary BECs in parallel and antiparallel magnetic fields. In sections 3.1 and 3.2, we summarize the formulation of reference [46]. In particular, we give an expression of the ground-state energy (equation (67)) in which a quantum correction due to zero-point fluctuations is included. In section 3.3, we use this formulation to derive expressions of the intercomponent ES and EE. Numerical results based on this formulation will be presented in section 4.

3.1. LLL magnetic Bloch states and Hamiltonian

We employ the LLL magnetic Bloch states $\{\Psi_{\mathbf{k}\alpha}(\mathbf{r})\}$ [22, 73–75] as a convenient single-particle basis for describing vortex lattices. The expressions of these states are shown in reference [46], and we summarize their main features in the following. Let \mathbf{a}_1 and \mathbf{a}_2 be the primitive vectors of a vortex lattice, and let \mathbf{K}_{α} be the pseudomomentum operator for a spin- α atom in a synthetic magnetic field B_{α} ($\alpha = \uparrow, \downarrow$). As expected for a ‘Bloch state’, $\Psi_{\mathbf{k}\alpha}(\mathbf{r})$ is an eigenstate of the magnetic translation $e^{-i\mathbf{K}_{\alpha} \cdot \mathbf{a}_j/\hbar}$ with an eigenvalue $e^{-i\mathbf{k} \cdot \mathbf{a}_j}$ ($j = 1, 2$). By taking N_v discrete wave vectors \mathbf{k} consistent with the boundary conditions of the system, $\{\Psi_{\mathbf{k}\alpha}(\mathbf{r})\}$ form a complete orthogonal basis of the LLL manifold⁹. Notably, $\Psi_{\mathbf{k}\alpha}(\mathbf{r})$ has a periodic pattern of zeros at [74]

$$\mathbf{r} = n_1 \mathbf{a}_1 + n_2 \mathbf{a}_2 + \frac{1}{2}(\mathbf{a}_1 + \mathbf{a}_2) - \epsilon_{\alpha} \ell^2 \mathbf{e}_z \times \mathbf{k}, \quad n_1, n_2 \in \mathbb{Z}. \quad (57)$$

Therefore, $\Psi_{\mathbf{k}\alpha}(\mathbf{r})$ represents a vortex lattice with primitive vectors \mathbf{a}_1 and \mathbf{a}_2 for any \mathbf{k} , and the locations of vortices (zeros) can be shifted by varying \mathbf{k} . Vortex lattices of binary BECs in figure 1 are obtained when spin- α bosons condense into $\Psi_{\mathbf{q}_{\alpha}\alpha}(\mathbf{r})$, where the wave vectors \mathbf{q}_{\uparrow} and \mathbf{q}_{\downarrow} are chosen in a way consistent with the displacement $u_1 \mathbf{a}_1 + u_2 \mathbf{a}_2$ between the components.

In the LLL approximation, the kinetic energy of each particle stays constant, and therefore we can focus on the interaction Hamiltonian H_{int} . Using the LLL magnetic Bloch states $\{\Psi_{\mathbf{k}\alpha}(\mathbf{r})\}$ as the basis, it is represented as

$$H_{\text{int}} = \frac{1}{2} \sum_{\alpha, \beta} \sum_{\mathbf{k}_1, \mathbf{k}_2, \mathbf{k}_3, \mathbf{k}_4} V_{\alpha\beta}(\mathbf{k}_1, \mathbf{k}_2, \mathbf{k}_3, \mathbf{k}_4) b_{\mathbf{k}_1\alpha}^{\dagger} b_{\mathbf{k}_2\beta}^{\dagger} b_{\mathbf{k}_3\beta} b_{\mathbf{k}_4\alpha}, \quad (58)$$

where $b_{\mathbf{k}\alpha}$ is a bosonic annihilation operator for the state $\Psi_{\mathbf{k}\alpha}(\mathbf{r})$ and

$$\begin{aligned} V_{\alpha\beta}(\mathbf{k}_1, \mathbf{k}_2, \mathbf{k}_3, \mathbf{k}_4) &= g_{\alpha\beta} \int d^2\mathbf{r} \Psi_{\mathbf{k}_1\alpha}^*(\mathbf{r}) \Psi_{\mathbf{k}_2\beta}^*(\mathbf{r}) \Psi_{\mathbf{k}_3\beta}(\mathbf{r}) \Psi_{\mathbf{k}_4\alpha}(\mathbf{r}). \end{aligned} \quad (59)$$

The expression of the interaction matrix element $V_{\alpha\beta}(\mathbf{k}_1, \mathbf{k}_2, \mathbf{k}_3, \mathbf{k}_4)$ that is convenient for numerical calculations is given in reference [46].

3.2. Bogoliubov approximation

We now apply the Bogoliubov approximation [18, 21, 22, 70], assuming that the condensation occurs at the wave vector \mathbf{q}_{α} in the spin- α component. To this end, it is useful to introduce

$$\tilde{b}_{\mathbf{k}\alpha} := b_{\mathbf{q}_{\alpha} + \mathbf{k}, \alpha}, \quad (60a)$$

$$\tilde{V}_{\alpha\beta}(\mathbf{k}_1, \mathbf{k}_2, \mathbf{k}_3, \mathbf{k}_4) := V_{\alpha\beta}(\mathbf{q}_{\alpha} + \mathbf{k}_1, \mathbf{q}_{\beta} + \mathbf{k}_2, \mathbf{q}_{\beta} + \mathbf{k}_3, \mathbf{q}_{\alpha} + \mathbf{k}_4). \quad (60b)$$

⁹In numerical calculations presented later, we set $\mathbf{k} = \frac{n_1}{N_{v1}} \mathbf{b}_1 + \frac{n_2}{N_{v2}} \mathbf{b}_2$ with $n_j \in \{0, 1, \dots, N_{v_j} - 1\}$ and $N_{v1} N_{v2} = N_v$. Here, \mathbf{b}_1 and \mathbf{b}_2 are the reciprocal primitive vectors as shown in figure 1.

By substituting

$$\tilde{b}_{\mathbf{0}\alpha} \simeq \tilde{b}_{\mathbf{0}\alpha}^\dagger \simeq \sqrt{N_\alpha - \sum_{\mathbf{k} \neq \mathbf{0}} \tilde{b}_{\mathbf{k}\alpha}^\dagger \tilde{b}_{\mathbf{k}\alpha}} \quad (61)$$

in equation (58) and retaining terms up to the second order in $\tilde{b}_{\mathbf{k}\alpha}$ and $\tilde{b}_{\mathbf{k}\alpha}^\dagger$ ($\mathbf{k} \neq \mathbf{0}$), we obtain the Bogoliubov Hamiltonian

$$H_{\text{int}} = \frac{1}{2} \sum_{\alpha,\beta} N_\alpha N_\beta \tilde{V}_{\alpha\beta}(\mathbf{0}, \mathbf{0}, \mathbf{0}, \mathbf{0}) - \frac{1}{2} \sum_{\mathbf{k} \neq \mathbf{0}} J(\mathbf{k}) + \frac{1}{2} \sum_{\mathbf{k} \neq \mathbf{0}} \left(\tilde{b}_{\mathbf{k}\uparrow}^\dagger, \tilde{b}_{\mathbf{k}\downarrow}^\dagger, \tilde{b}_{-\mathbf{k}\uparrow}, \tilde{b}_{-\mathbf{k}\downarrow} \right) \mathcal{M}(\mathbf{k}) \begin{pmatrix} \tilde{b}_{\mathbf{k}\uparrow} \\ \tilde{b}_{\mathbf{k}\downarrow} \\ \tilde{b}_{-\mathbf{k}\uparrow}^\dagger \\ \tilde{b}_{-\mathbf{k}\downarrow}^\dagger \end{pmatrix}, \quad (62)$$

where

$$J(\mathbf{k}) := \sum_{\alpha,\beta} N_\beta \left[\tilde{V}_{\alpha\beta}(\mathbf{k}, \mathbf{0}, \mathbf{0}, \mathbf{k}) - \tilde{V}_{\alpha\beta}(\mathbf{0}, \mathbf{0}, \mathbf{0}, \mathbf{0}) \right] + \sum_\alpha N_\alpha \tilde{V}_{\alpha\alpha}(\mathbf{k}, \mathbf{0}, \mathbf{k}, \mathbf{0}), \quad (63)$$

and the expression of the 4×4 matrix $\mathcal{M}(\mathbf{k})$ is shown in reference [46].

To diagonalize equation (62), we perform the Bogoliubov transformation

$$\begin{pmatrix} \tilde{b}_{\mathbf{k}\uparrow} \\ \tilde{b}_{\mathbf{k}\downarrow} \\ \tilde{b}_{-\mathbf{k}\uparrow}^\dagger \\ \tilde{b}_{-\mathbf{k}\downarrow}^\dagger \end{pmatrix} = W(\mathbf{k}) \begin{pmatrix} \gamma_{\mathbf{k},1} \\ \gamma_{\mathbf{k},2} \\ \gamma_{-\mathbf{k},1}^\dagger \\ \gamma_{-\mathbf{k},2}^\dagger \end{pmatrix}, \quad (64a)$$

$$W(\mathbf{k}) = \begin{pmatrix} \mathcal{U}(\mathbf{k}) & \mathcal{V}^*(-\mathbf{k}) \\ \mathcal{V}(\mathbf{k}) & \mathcal{U}^*(-\mathbf{k}) \end{pmatrix}. \quad (64b)$$

Here, the paraunitary matrix $W(\mathbf{k})$ is chosen to satisfy

$$\begin{aligned} \tau_3 \mathcal{M}(\mathbf{k}) W(\mathbf{k}) &= W(\mathbf{k}) \text{diag}(E_1(\mathbf{k}), E_2(\mathbf{k}), -E_1(-\mathbf{k}), -E_2(-\mathbf{k})), \end{aligned} \quad (65)$$

where $\tau_3 := \text{diag}(1, 1, -1, -1)$. Namely, $W(\mathbf{k})$ and $E_j(\mathbf{k})$ ($j = 1, 2$) are obtained by solving the right eigenvalue problem of $\tau_3 \mathcal{M}(\mathbf{k})$. Equation (62) is then diagonalized as

$$\begin{aligned} H_{\text{int}} &= \frac{1}{2} \sum_{\alpha,\beta} N_\alpha N_\beta \tilde{V}_{\alpha\beta}(\mathbf{0}, \mathbf{0}, \mathbf{0}, \mathbf{0}) - \frac{1}{2} \sum_{\mathbf{k} \neq \mathbf{0}} J(\mathbf{k}) \\ &+ \sum_{\mathbf{k} \neq \mathbf{0}} \sum_{j=1,2} E_j(\mathbf{k}) \left(\gamma_{\mathbf{k}j}^\dagger \gamma_{\mathbf{k}j} + \frac{1}{2} \right). \end{aligned} \quad (66)$$

We thus find that the Bogoliubov excitations (bogolons) are created by $\gamma_{\mathbf{k}j}^\dagger$ ($j = 1, 2$) and have the dispersion relations $\{E_j(\mathbf{k})\}$.

The ground state of equation (66) is given by the bogolon vacuum $|0\rangle$, which is specified by the condition that $\gamma_{\mathbf{k}j} |0\rangle = 0$ for all $\mathbf{k} \neq \mathbf{0}$ and $j = 1, 2$. The ground-state energy E_{GS} (scaled

by the interaction energy scale gn^2A) is therefore given by

$$\begin{aligned} \frac{E_{\text{GS}}}{gn^2A} &= \frac{1}{2} \sum_{\alpha,\beta} \frac{A}{g} \tilde{V}_{\alpha\beta}(\mathbf{0}, \mathbf{0}, \mathbf{0}, \mathbf{0}) \\ &+ \frac{1}{gn\nu N_v} \sum_{\mathbf{k} \neq \mathbf{0}} \left[\sum_j E_j(\mathbf{k}) - J(\mathbf{k}) \right] \\ &= \frac{1}{2} \sum_{\alpha,\beta} \frac{A}{g} \tilde{V}_{\alpha\beta}(\mathbf{0}, \mathbf{0}, \mathbf{0}, \mathbf{0}) \\ &+ \frac{1}{2\pi gn\nu} \int_{\text{BZ}} d^2\mathbf{k} \ell^2 \left[\sum_j E_j(\mathbf{k}) - J(\mathbf{k}) \right]. \end{aligned} \quad (67)$$

Here, in the final expression, we take the thermodynamic limit $N_v \rightarrow \infty$ so that the sum is replaced by the integral over the Brillouin zone as $\frac{1}{N_v} \sum_{\mathbf{k} \neq \mathbf{0}} \rightarrow \frac{1}{|\mathbf{b}_1 \times \mathbf{b}_2|} \int d^2\mathbf{k} = \frac{1}{2\pi} \int_{\text{BZ}} d^2\mathbf{k} \ell^2$; this integral is convergent as the integrand is finite over the entire Brillouin zone. The first term on the right-hand side of equation (67) corresponds to the mean-field ground-state energy, which has been analyzed by Mueller and Ho [36]. The other term gives a quantum correction and is inversely proportional to the filling factor ν . In section 4.5, we numerically calculate equation (67), and discuss how the quantum correction affects the ground-state phase diagrams.

Using equation (64), we can calculate the following correlators in the ground state:

$$\langle 0 | \tilde{b}_{\mathbf{k},\alpha}^\dagger \tilde{b}_{\mathbf{k},\alpha} | 0 \rangle = \sum_j |\mathcal{V}_{\alpha,j}(-\mathbf{k})|^2, \quad (68a)$$

$$\langle 0 | \tilde{b}_{-\mathbf{k},\alpha} \tilde{b}_{-\mathbf{k},\alpha}^\dagger | 0 \rangle = \sum_j |\mathcal{U}_{\alpha,j}(-\mathbf{k})|^2, \quad (68b)$$

$$\langle 0 | \tilde{b}_{-\mathbf{k},\alpha} \tilde{b}_{\mathbf{k},\alpha} | 0 \rangle = \sum_j \mathcal{U}_{\alpha,j}(-\mathbf{k}) \mathcal{V}_{\alpha,j}^*(-\mathbf{k}), \quad (68c)$$

$$\langle 0 | \tilde{b}_{\mathbf{k},\alpha}^\dagger \tilde{b}_{-\mathbf{k},\alpha}^\dagger | 0 \rangle = \sum_j \mathcal{U}_{\alpha,j}^*(-\mathbf{k}) \mathcal{V}_{\alpha,j}(-\mathbf{k}). \quad (68d)$$

Here, we have nonzero ‘anomalous’ correlators in equations (68c) and (68d) as the particle numbers N_\uparrow and N_\downarrow are not conserved in the Bogoliubov Hamiltonian (62). Using equations (68a) and (68b), we can further calculate the fraction of depletion n'/n , which is equal for the two components, as

$$\begin{aligned} \frac{n'}{n} &= \frac{1}{N_\alpha} \sum_{\mathbf{k} \neq \mathbf{0}} \langle 0 | \tilde{b}_{\mathbf{k},\alpha}^\dagger \tilde{b}_{\mathbf{k},\alpha} | 0 \rangle \\ &= \frac{2}{\nu N_v} \sum_{\mathbf{k} \neq \mathbf{0}} \sum_{j=1,2} |\mathcal{V}_{\alpha,j}(-\mathbf{k})|^2 \quad (\alpha = \uparrow, \downarrow). \end{aligned} \quad (69)$$

As discussed in section 2.6 (see equation (56)), this quantity is expected to diverge logarithmically as a function of N_v . We will confirm this behavior numerically in section 4.4. This diverging behavior comes from the divergence of $|\mathcal{V}_{\alpha,2}(-\mathbf{k})|^2$ for $\mathbf{k} \rightarrow \mathbf{0}$ in equation (69). We note that the Bogoliubov theory should be applied under the condition of weak depletion $n'/n \ll 1$; this condition is satisfied in typical experiments of ultracold atomic gases, where N_v is at most of the order of 100 [12].

3.3. Intercomponent entanglement

For the RDM ρ_{\uparrow} for the spin- \uparrow component, we introduce the following Gaussian ansatz [62, 63, 67, 68]:

$$\rho_{\uparrow} = \frac{1}{Z_e} e^{-H_e}, \quad Z_e = \text{Tr } e^{-H_e}, \quad (70a)$$

$$H_e = \frac{1}{2} \sum_{\mathbf{k} \neq 0} \left(\tilde{b}_{\mathbf{k},\uparrow}^\dagger, \tilde{b}_{-\mathbf{k},\uparrow} \right) M_e(\mathbf{k}) \begin{pmatrix} \tilde{b}_{\mathbf{k},\uparrow} \\ \tilde{b}_{-\mathbf{k},\uparrow}^\dagger \end{pmatrix}, \quad (70b)$$

with

$$M_e(\mathbf{k}) = \begin{pmatrix} h_{\mathbf{k}} & -\lambda_{\mathbf{k}} \\ -\lambda_{-\mathbf{k}}^* & h_{-\mathbf{k}} \end{pmatrix}, \quad \lambda_{\mathbf{k}} = \lambda_{-\mathbf{k}}. \quad (71)$$

By performing a Bogoliubov transformation

$$\begin{pmatrix} \tilde{b}_{\mathbf{k},\uparrow} \\ \tilde{b}_{-\mathbf{k},\uparrow}^\dagger \end{pmatrix} = W_e(\mathbf{k}) \begin{pmatrix} \eta_{\mathbf{k}} \\ \eta_{-\mathbf{k}}^\dagger \end{pmatrix}, \quad (72a)$$

$$W_e(\mathbf{k}) = \begin{pmatrix} \cosh \theta_{\mathbf{k}} & e^{-i\phi_{\mathbf{k}}} \sinh \theta_{\mathbf{k}} \\ e^{i\phi_{\mathbf{k}}} \sinh \theta_{\mathbf{k}} & \cosh \theta_{\mathbf{k}} \end{pmatrix} \quad (72b)$$

with

$$\cosh 2\theta_{\mathbf{k}} = \frac{h_{\mathbf{k}} + h_{-\mathbf{k}}}{2\tilde{h}_{\mathbf{k}}}, \quad e^{-i\phi_{\mathbf{k}}} \sinh 2\theta_{\mathbf{k}} = \frac{\lambda_{\mathbf{k}}}{\tilde{h}_{\mathbf{k}}}, \quad (73a)$$

$$\tilde{h}_{\mathbf{k}} = \sqrt{\frac{1}{4}(h_{\mathbf{k}} + h_{-\mathbf{k}})^2 - |\lambda_{\mathbf{k}}|^2}, \quad (73b)$$

the entanglement Hamiltonian in H_e in equation (70) is diagonalized as

$$\begin{aligned} H_e &= \frac{1}{2} \sum_{\mathbf{k} \neq 0} \left(\xi_{\mathbf{k}} \eta_{\mathbf{k}}^\dagger \eta_{\mathbf{k}} + \xi_{-\mathbf{k}} \eta_{-\mathbf{k}} \eta_{-\mathbf{k}}^\dagger \right) \\ &= \sum_{\mathbf{k} \neq 0} \xi_{\mathbf{k}} \left(\eta_{\mathbf{k}}^\dagger \eta_{\mathbf{k}} + \frac{1}{2} \right), \end{aligned} \quad (74)$$

where

$$\xi_{\mathbf{k}} := \tilde{h}_{\mathbf{k}} + \frac{h_{\mathbf{k}} - h_{-\mathbf{k}}}{2} \quad (75)$$

is the single-particle ES.

Using the relation (72) and the Bose distribution functions

$$\text{Tr} \left(\eta_{\mathbf{k}}^\dagger \eta_{\mathbf{k}} \rho_{\uparrow} \right) = \frac{1}{e^{\xi_{\mathbf{k}}} - 1} = f_B(\xi_{\mathbf{k}}), \quad (76a)$$

$$\text{Tr} \left(\eta_{-\mathbf{k}} \eta_{-\mathbf{k}}^\dagger \rho_{\uparrow} \right) = 1 + f_B(\xi_{-\mathbf{k}}) = -f_B(-\xi_{-\mathbf{k}}), \quad (76b)$$

we obtain

$$\text{Tr} \left(\tilde{b}_{\mathbf{k},\uparrow}^\dagger \tilde{b}_{\mathbf{k},\uparrow} \rho_{\uparrow} \right) = f_B(\xi_{\mathbf{k}}) \cosh^2 \theta_{\mathbf{k}} - f_B(-\xi_{-\mathbf{k}}) \sinh^2 \theta_{\mathbf{k}}, \quad (77a)$$

$$\text{Tr} \left(\tilde{b}_{-\mathbf{k},\uparrow} \tilde{b}_{-\mathbf{k},\uparrow}^\dagger \rho_{\uparrow} \right) = -f_B(-\xi_{-\mathbf{k}}) \cosh^2 \theta_{\mathbf{k}} + f_B(\xi_{\mathbf{k}}) \sinh^2 \theta_{\mathbf{k}}, \quad (77b)$$

$$2 \text{Tr} \left(\tilde{b}_{-\mathbf{k},\uparrow} \tilde{b}_{\mathbf{k},\uparrow} \rho_{\uparrow} \right) = [f_B(\xi_{\mathbf{k}}) - f_B(-\xi_{-\mathbf{k}})] e^{-i\phi_{\mathbf{k}}} \sinh(2\theta_{\mathbf{k}}). \quad (77c)$$

We require these to be equal to the correlators (68) with respect to the Bogoliubov ground state. We can then express $f_B(\xi_{\mathbf{k}})$ in terms of the correlators (68) in the following way. First, by taking the sum and the difference of equations (77a) and (77b), we have

$$\langle \tilde{b}_{\mathbf{k},\uparrow}^\dagger \tilde{b}_{\mathbf{k},\uparrow} \rangle + \langle \tilde{b}_{-\mathbf{k},\uparrow} \tilde{b}_{-\mathbf{k},\uparrow}^\dagger \rangle = [f_B(\xi_{\mathbf{k}}) - f_B(-\xi_{-\mathbf{k}})] \cosh(2\theta_{\mathbf{k}}), \quad (78a)$$

$$\langle \tilde{b}_{\mathbf{k},\uparrow}^\dagger \tilde{b}_{\mathbf{k},\uparrow} \rangle - \langle \tilde{b}_{-\mathbf{k},\uparrow} \tilde{b}_{-\mathbf{k},\uparrow}^\dagger \rangle = f_B(\xi_{\mathbf{k}}) + f_B(-\xi_{-\mathbf{k}}), \quad (78b)$$

where we take the shorthand notation $\langle \cdot \rangle := \langle 0 | \cdot | 0 \rangle$. Next, using equations (77c) and (78a), we have

$$\begin{aligned} f_B(\xi_{\mathbf{k}}) - f_B(-\xi_{-\mathbf{k}}) \\ = \sqrt{\left(\langle \tilde{b}_{\mathbf{k},\uparrow}^\dagger \tilde{b}_{\mathbf{k},\uparrow} \rangle + \langle \tilde{b}_{-\mathbf{k},\uparrow} \tilde{b}_{-\mathbf{k},\uparrow}^\dagger \rangle \right)^2 - 4 \left| \langle \tilde{b}_{-\mathbf{k},\uparrow} \tilde{b}_{\mathbf{k},\uparrow} \rangle \right|^2}. \end{aligned} \quad (79)$$

Lastly, using equations (78b) and (79), we obtain

$$\begin{aligned} f_B(\xi_{\mathbf{k}}) &= \frac{1}{2} \left(\langle \tilde{b}_{\mathbf{k},\uparrow}^\dagger \tilde{b}_{\mathbf{k},\uparrow} \rangle - \langle \tilde{b}_{-\mathbf{k},\uparrow} \tilde{b}_{-\mathbf{k},\uparrow}^\dagger \rangle \right) \\ &+ \sqrt{\frac{1}{4} \left(\langle \tilde{b}_{\mathbf{k},\uparrow}^\dagger \tilde{b}_{\mathbf{k},\uparrow} \rangle + \langle \tilde{b}_{-\mathbf{k},\uparrow} \tilde{b}_{-\mathbf{k},\uparrow}^\dagger \rangle \right)^2 - \left| \langle \tilde{b}_{-\mathbf{k},\uparrow} \tilde{b}_{\mathbf{k},\uparrow} \rangle \right|^2}, \end{aligned} \quad (80)$$

from which we can calculate the single-particle ES $\xi_{\mathbf{k}} = \ln [1 + f_B(\xi_{\mathbf{k}})^{-1}]$.

We can further use equation (80) to calculate the intercomponent EE as

$$S_e = \sum_{\mathbf{k} \neq 0} \left\{ -f_B(\xi_{\mathbf{k}}) \ln f_B(\xi_{\mathbf{k}}) + [1 + f_B(\xi_{\mathbf{k}})] \ln [1 + f_B(\xi_{\mathbf{k}})] \right\}. \quad (81)$$

As discussed in section 2.5 (see equation (50)), S_e is expected to show a volume-law behavior with a subleading logarithmic correction. The EE per flux quantum in the thermodynamic limit is then expressed in the integral form

$$\begin{aligned} \lim_{N_v \rightarrow \infty} \frac{S_e}{N_v} &= \frac{1}{2\pi} \int_{BZ} d^2 \mathbf{k} \ell^2 \left\{ -f_B(\xi_{\mathbf{k}}) \ln f_B(\xi_{\mathbf{k}}) \right. \\ &\quad \left. + [1 + f_B(\xi_{\mathbf{k}})] \ln [1 + f_B(\xi_{\mathbf{k}})] \right\}. \end{aligned} \quad (82)$$

We note that the correlators (68) are independent of ν once the lattice structure is fixed. Therefore, the EE per flux quantum in equation (82) is also independent of ν in a similar manner. In section 4.3, we will calculate the EE per flux quantum by assuming the structure in the mean-field ground state.

4. Numerical results

In this section, we present numerical results that are obtained using the Bogoliubov theory of section 3. In this formulation, one starts from the lattice structure with the primitive vectors \mathbf{a}_1 and \mathbf{a}_2 and the displacement parameters u_1

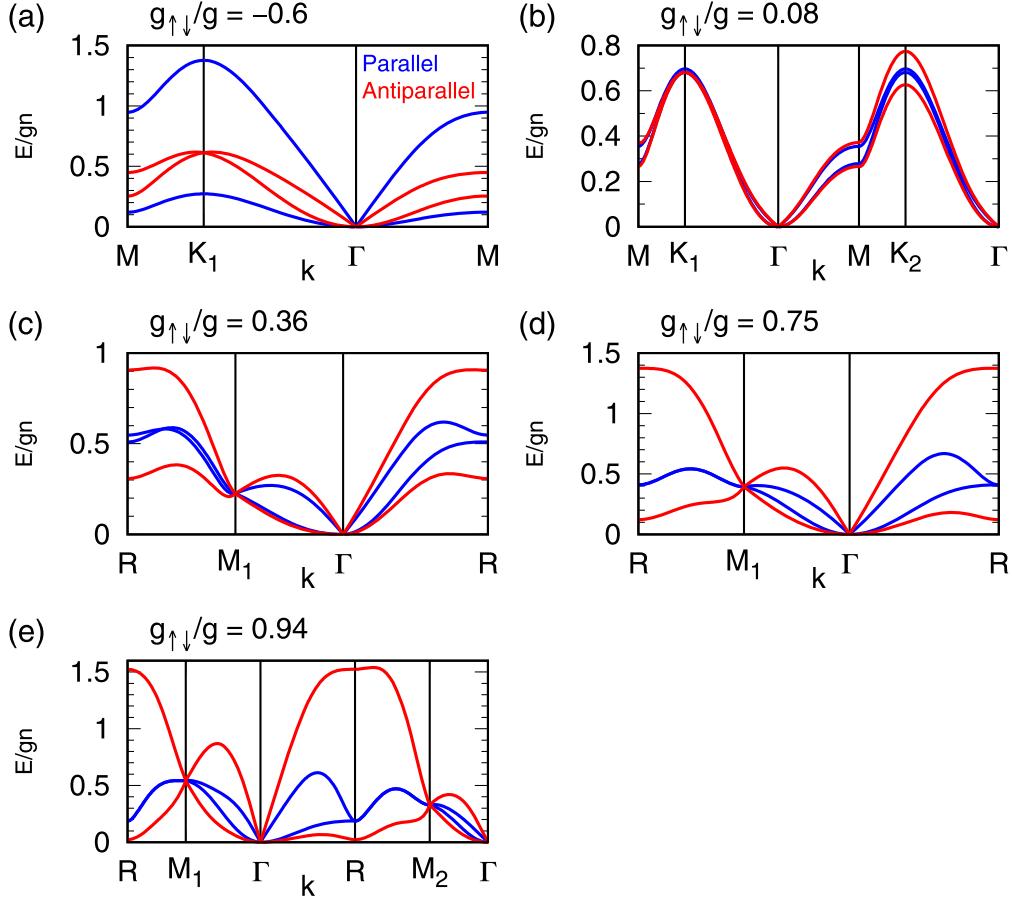


Figure 3. Bogoliubov excitation spectra $\{E_j(\mathbf{k})\}$ (in units of gn) for different values of $g_{\uparrow\downarrow}/g$ corresponding to the lattice structures (a)–(e) shown in figure 1. In each panel, both results for parallel (blue) and antiparallel (red) magnetic fields are shown. Calculations are done along the dotted arrows in the lower panels of figure 1.

and u_2 (see figure 1(f)). In the GP mean-field theory, these parameters are determined so as to minimize the mean-field ground-state energy (the first term on the right-hand side of equation (67)) for a fixed magnetic length ℓ . As demonstrated by Mueller and Ho [36], this mean-field analysis gives a rich phase diagram that consists of five different vortex-lattice phases as shown in figure 1. In sections 4.1–4.4, we analyze renormalized coupling constants, excitation spectra, intercomponent entanglement, and the fraction of depletion, respectively, using the Bogoliubov theory based on the mean-field vortex lattice structures. Therefore, the results in these sections correspond to the case of $\nu = \infty$. As we lower the filling factor ν , quantum fluctuations are expected to affect the vortex lattice structures and the ground-state phase diagrams. In section 4.5, we investigate how quantum fluctuations affect the ground-state phase diagrams for parallel and antiparallel fields by calculating a quantum correction to the ground-state energy (i.e., the term proportional to ν^{-1} in equation (67)).

4.1. Renormalized coupling constants

We first determine the renormalized coupling constants $\bar{g}_{\alpha\beta}$ or equivalently, the renormalization factors $\beta_{\alpha\beta} := \bar{g}_{\alpha\beta}/g_{\alpha\beta}$ that are introduced in section 2.2. Comparing the mean-field ground-state energy (the first term of equation (67)) with the

corresponding field-theoretical expression (11), we find

$$\begin{aligned} \bar{g}_{\alpha\beta} &= \beta_{\alpha\beta} g_{\alpha\beta} = A V_{\alpha\beta}(\mathbf{q}_\alpha, \mathbf{q}_\beta, \mathbf{q}_\beta, \mathbf{q}_\alpha) \\ &= A g_{\alpha\beta} \int d^2\mathbf{r} |\Psi_{\mathbf{q}_\alpha, \alpha}(\mathbf{r})|^2 |\Psi_{\mathbf{q}_\beta, \beta}(\mathbf{r})|^2. \end{aligned} \quad (83)$$

This expression can also be obtained by substituting the condensate wave function $\sqrt{N_\alpha} \Psi_{\mathbf{q}_\alpha, \alpha}(\mathbf{r})$ into $\psi_\alpha(\mathbf{r})$ in equation (6). As seen in this expression, $\bar{g}_{\alpha\beta}$ is determined from the contribution of each interaction term to the mean-field ground-state energy.

Figure 2 shows the renormalization factors $\beta := \beta_{\uparrow\uparrow} = \beta_{\downarrow\downarrow}$ and $\beta_{\uparrow\downarrow} = \beta_{\downarrow\uparrow}$ calculated for the mean-field vortex lattice structures. For overlapping triangular, interlaced triangular, and square lattices, β and $\beta_{\uparrow\downarrow}$ do not depend on $g_{\uparrow\downarrow}/g$ as the lattice structures remain unchanged in the concerned regions. For rhombic and rectangular lattices, in contrast, β and $\beta_{\uparrow\downarrow}$ do depend on $g_{\uparrow\downarrow}/g$ as the inner angle θ and the aspect ratio b/a continuously vary for the former and latter lattices, respectively.

We have argued in section 2.2 that the intracomponent coupling is always enhanced by the renormalization. We indeed find $\beta > 1$ in all the regions in figure 2. We have also argued that the intercomponent repulsion $g_{\uparrow\downarrow} > 0$ (attraction $g_{\uparrow\downarrow} < 0$) is reduced (enhanced) by the renormalization owing

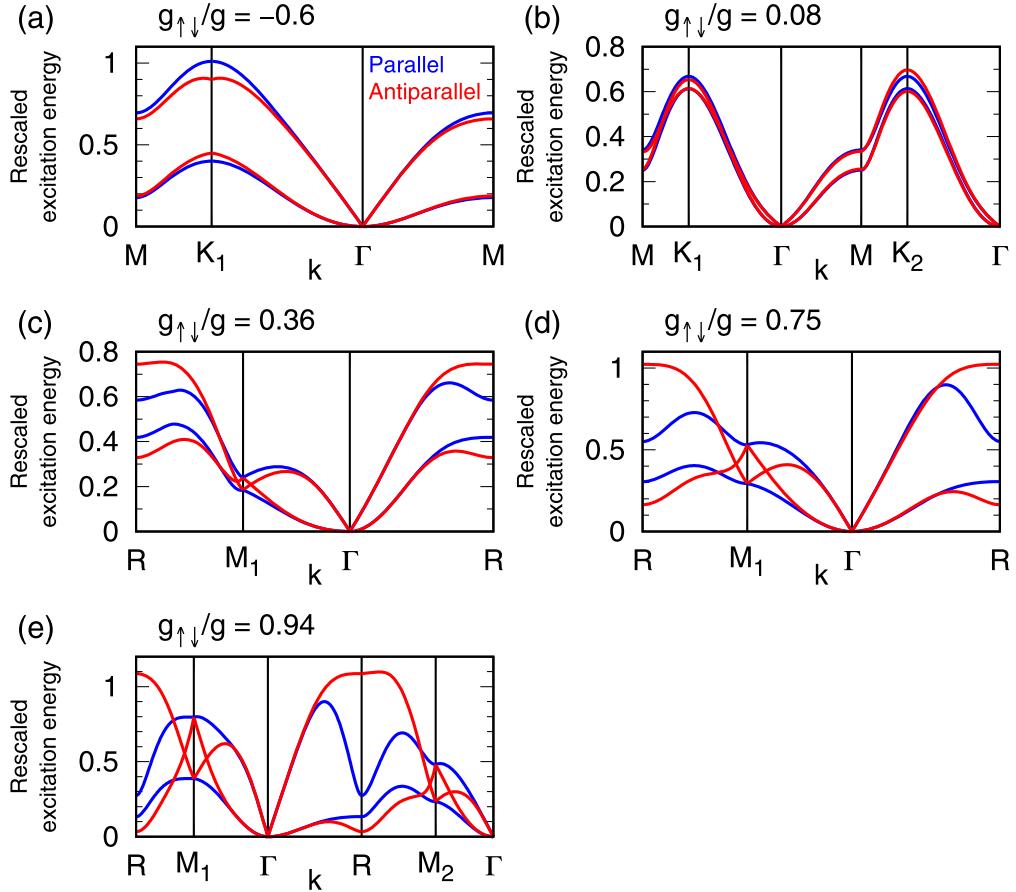


Figure 4. Rescaled Bogoliubov excitation spectra for the five cases (a)–(e) shown in figure 3. Blue curves show $E_1^P(\mathbf{k})/(\sqrt{g\bar{g}_-}n)$ and $E_2^P(\mathbf{k})/(\sqrt{g\bar{g}_+}n)$ for parallel (P) fields while red curves show $E_1^{AP}(\mathbf{k})/(\sqrt{g\bar{g}_+}n)$ and $E_2^{AP}(\mathbf{k})/(\sqrt{g\bar{g}_-}n)$ for antiparallel (AP) fields. Here, $E_j^{P/AP}(\mathbf{k})$ with $j = 1$ and 2 correspond to the upper and lower excitation bands, respectively. We can confirm that the blue and red curves overlap at sufficiently low energies around the Γ point, which indicates the rescaling relations in equation (36).

to the displacement (overlap) of vortices between the components. In figure 2, we indeed find $\beta_{\uparrow\downarrow} < 1$ ($\beta_{\uparrow\downarrow} > 1$) for $g_{\uparrow\downarrow} > 0$ ($g_{\uparrow\downarrow} < 0$). Furthermore, β ($\beta_{\uparrow\downarrow}$) monotonically increases (decreases) as a function of $g_{\uparrow\downarrow}/g$ for $g_{\uparrow\downarrow} > 0$. This reflects the fact that with increasing $g_{\uparrow\downarrow}/g$, vortices in different components tend to repel more strongly with each other at the cost of increasing the intracomponent interaction energy.

4.2. Excitation spectrum and elastic constants

As explained in section 3.2 (see equation (65)), the excitation spectrum $E_j(\mathbf{k})$ ($j = 1, 2$) can be obtained by numerically calculating the right eigenvalues of the 4×4 matrix $\tau_3 \mathcal{M}(\mathbf{k})$. Figure 3 presents spectra obtained in this way for all the lattice structures (a)–(e) shown in figure 1 and for both parallel and antiparallel fields. In reference [46],¹⁰ we discuss various unique features of these spectra such as linear and quadratic dispersion relations at low energies and the

emergence of line and point nodes at high energies that are related to a fractional translation symmetry. Here, we aim to demonstrate the rescaling relations in equations (36) and (37) which are predicted by the low-energy effective field theory. In reference [46], the unrenormalized coupling constants $g_{\alpha\beta}$ are used for the rescaling, which leads to an incorrect conclusion that the rescaling relations hold only for overlapping triangular lattices. Using the renormalized coupling constants obtained in section 4.1, we can demonstrate the rescaling relations for all the five structures (a)–(e) shown in figure 1.

Figure 4 displays rescaled excitation spectra for the five cases (a)–(e) in figure 3. Here, $\bar{g}_{\pm} := \bar{g} \pm \bar{g}_{\uparrow\downarrow} = \beta g \pm \beta_{\uparrow\downarrow} g_{\uparrow\downarrow}$ are used for the rescaling, where the renormalization factors β and $\beta_{\uparrow\downarrow}$ are shown in figure 2. We can confirm that the rescaling relations in equation (36) hold at sufficiently low energies around the Γ point. Interestingly, in figures 4(a) and (b), the rescaling relations hold approximately up to high energies, which is beyond the scope of effective field theory. At low energies, the spectra in figure 3 can be fit well by linear and quadratic dispersion relations

$$E_j(\mathbf{k}) = \sqrt{2}gn(k\ell)^j f_j(\varphi) \quad (j = 1, 2), \quad (84)$$

¹⁰ There are errors in the scales of some figures in reference [46]. Specifically, the numerical data for the vertical axes in figures 2, 4, and 5 should be multiplied by $1/4$, $1/(2\sqrt{2})$, and $1/8$, respectively. These errors are unrelated to the issue of renormalization discussed in the present paper. As our understanding of the rescaling relations is now updated from reference [46], figures 3, 5, and 6 of the present paper could be seen as improved versions of these figures.

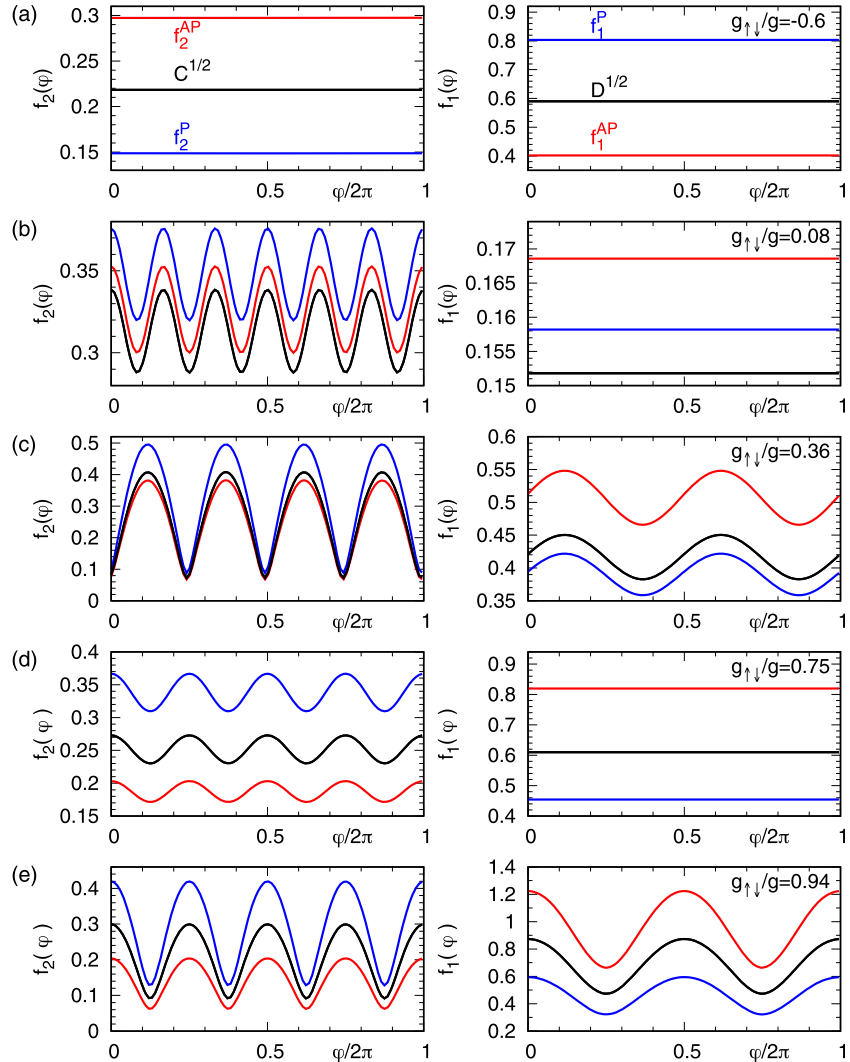


Figure 5. Dimensionless functions $f_2^{P/AP}(\varphi)$ (left) and $f_1^{P/AP}(\varphi)$ (right) for parallel (P; blue) and antiparallel (AP; red) fields for the same cases (a)–(e) as in figures 3 and 4. These functions express the anisotropy of the low-energy spectra as in equation (84), and they are calculated from the $\{E_j(\mathbf{k})\}$ along a circular path $\mathbf{k} = k(\cos \varphi, \sin \varphi)$ with $k = 0.001a/\ell^2$ and $\varphi \in [0, 2\pi]$. With proper rescaling as in equation (37), the curves for parallel and antiparallel fields are found to agree perfectly up to numerical precision. Specifically, in the left panels, $f_2^P(\varphi)\sqrt{g/g_+}$ and $f_2^{AP}(\varphi)\sqrt{g/g_-}$ give the common function $\sqrt{C(\varphi)}$ (black). In the right panels, $f_1^P(\varphi)\sqrt{g/g_-}$ and $f_1^{AP}(\varphi)\sqrt{g/g_+}$ give the common function $\sqrt{D(\varphi)}$ (black).

where the wave vector is parametrized as $\mathbf{k} = k(\cos \varphi, \sin \varphi)$ and $\{f_j(\varphi)\}$ are dimensionless functions that characterize the anisotropy of the spectrum. Figure 5 shows the functions $\{f_j(\varphi)\}$ obtained numerically for the same cases as in figures 3 and 4. We find that with proper rescaling as in equation (37), the curves for parallel and antiparallel fields coincide perfectly up to numerical precision, giving the functions $\sqrt{C(\varphi)}$ and $\sqrt{D(\varphi)}$ that are related to the elastic constants.

By comparing the obtained $\sqrt{C(\varphi)}$ and $\sqrt{D(\varphi)}$ with the analytical expressions in equation (33), we can determine the dimensionless elastic constants $\{C_i\}$ and $\{D_i\}$. Figure 6 shows the determined elastic constants as functions of $g_{\uparrow\downarrow}/g$, which are common for parallel and antiparallel fields. In our previous work [46], we obtained different elastic constants for the two types of fields as we missed the necessity of using the renormalized coupling constants in relating the spectra to the elastic constants. Figure 6 is essentially consistent with the

elastic constants determined by a different method by Keçeli and Oktel [45] except that the constant C_4 for interlaced triangular lattices (b) was overlooked in reference [45].

4.3. Intercomponent entanglement spectrum and entropy

Here we present numerical results on the intercomponent ES and EE in the Bogoliubov ground state. Calculations are based on the formulation in section 3.3. The obtained results are compared with the field-theoretical results in section 2.5.

The left panels of figure 7 display the single-particle ES $\xi_{\mathbf{k}}$ for the same cases as in figures 3–5. Around the Γ point, $\xi_{\mathbf{k}}$ can be well fitted by the square-root dispersion relation

$$\xi_{\mathbf{k}} = c(\varphi)\sqrt{kl} \quad (85)$$

for $\mathbf{k} = k(\cos \varphi, \sin \varphi)$, where $c(\varphi)$ is a dimensionless function that expresses the anisotropy. The right panels of figure 7

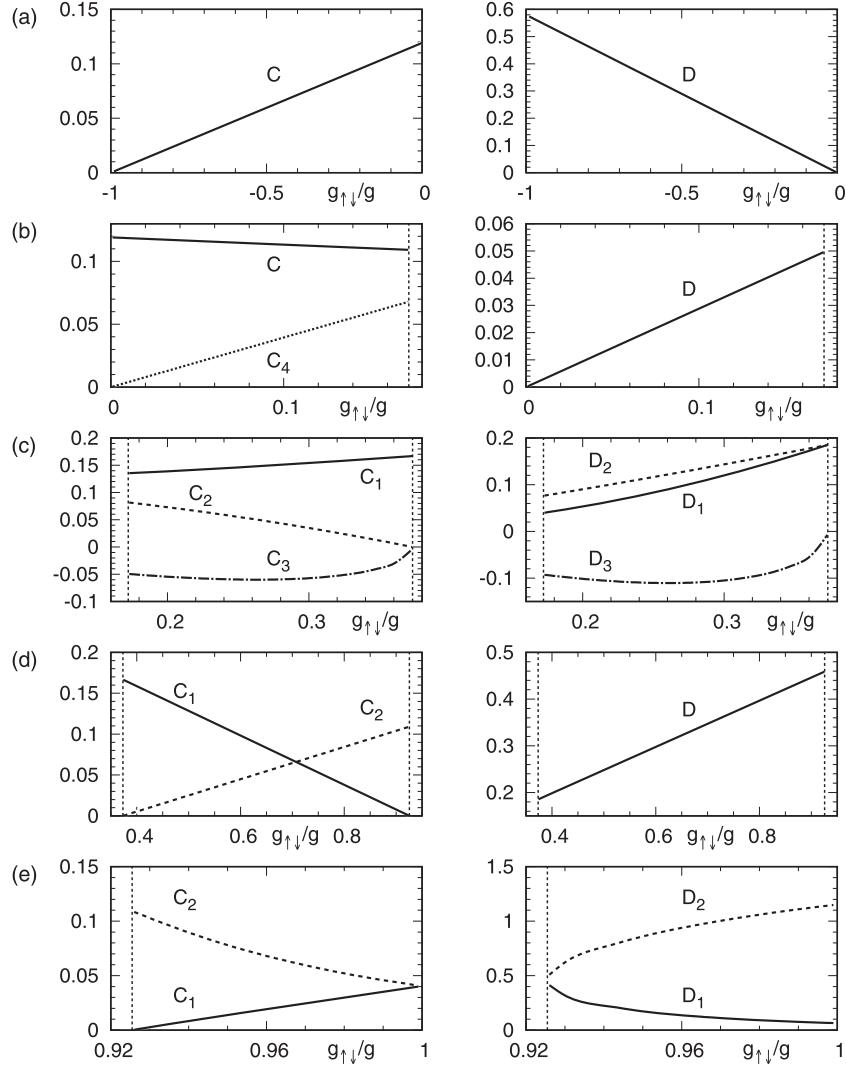


Figure 6. Dimensionless elastic constants C_i ($i = 1, 2, 3, 4$) (left) and D_i ($i = 1, 2, 3$) (right) for the lattice structures (a)–(e) shown in figure 1. These constants are obtained by fitting the numerically obtained functions $\sqrt{C(\varphi)}$ and $\sqrt{D(\varphi)}$ (common for parallel and antiparallel fields as shown in figure 5) using equation (33). See equation (15) for the symmetry constraints on the constants. Vertical dashed lines indicate the transition points in the mean-field ground state.

show the function $c(\varphi)$ determined from the data of $\xi_{\mathbf{k}}$ along a circular path around the Γ point. With proper rescaling, the curves for parallel and antiparallel fields are found to coincide perfectly up to numerical precision; furthermore, the rescaled curves are found to agree accurately with $4[C(\varphi)/D(\varphi)]^{1/2}$ (not shown), where $\sqrt{C(\varphi)}$ and $\sqrt{D(\varphi)}$ are shown in figure 5. Thus, we can confirm the rescaling relation for the entanglement spectra in equation (46).

In the left panels of figure 7, we also find that $\xi_{\mathbf{k}}$ diverges at some high-symmetry points and along lines in the Brillouin zone. For square (d) and rectangular (e) lattices in antiparallel fields, in particular, divergence occurs along the edges of the Brillouin zone. In our previous work [46] (see appendix D therein), it has been found that at the M_1 and M_2 points for rhombic, square and rectangular lattices and for both parallel and antiparallel fields, the Bogoliubov Hamiltonian matrix $\mathcal{M}(\mathbf{k})$ has the structure in which the spin- \uparrow and \downarrow components are decoupled. Therefore, $\xi_{\mathbf{k}}$ naturally diverges at these points. However, we have not been able to find such a simple structure

of $\mathcal{M}(\mathbf{k})$ along the edges of the Brillouin zone for square (d) and rectangular (e) lattices in antiparallel fields.

Figure 8(a) shows the intercomponent EE per flux quantum as a function of the ratio $g_{\uparrow\downarrow}/g$ for parallel (blue) and antiparallel (red) fields. We find that for repulsive (attractive) $g_{\uparrow\downarrow}$, the EE tends to be larger for parallel (antiparallel) fields, in consistency with the field-theoretical result in section 2.5 (see equation (51)). This behavior is in qualitative agreement with the exact diagonalization results in a quantum (spin) Hall regime with $\nu = \mathcal{O}(1)$ [42, 52], in which product states of nearly uncorrelated quantum Hall states are found to be robust for an intercomponent attraction (repulsion) in the case of parallel (antiparallel) fields.

In figure 8(b), we examine the scaling of the intercomponent EE S_e as a function of N_v . As seen in this figure, the dominant part of the scaling is given by a volume-law behavior $\alpha_1 N_v$; such a volume-law contribution is standard for an extensive cut as discussed here, and has also been found elsewhere [62, 63, 76–78]. In agreement with the field-theoretical

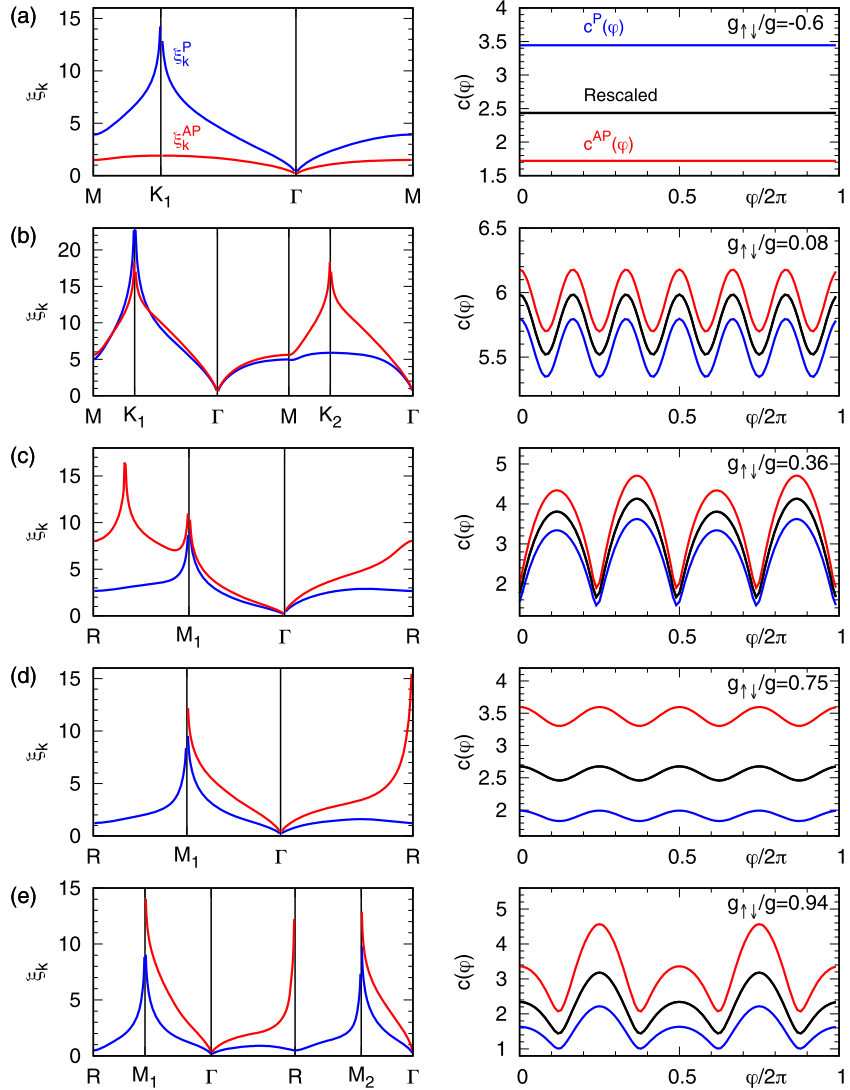


Figure 7. (Left panels) Single-particle ES $\xi_k^{P/AP}$ for parallel (P; blue) and antiparallel (AP; red) fields for the same cases (a)–(e) as in figures 3–5. Calculations are based on equation (80) and done along the paths indicated by dotted arrows shown in the lower panels of figure 1. The spectra ξ_k show divergence at some high-symmetry points and along lines in the first Brillouin zone. In (d) and (e), in particular, divergence occurs along the edges of the Brillouin zone for antiparallel fields, and thus the value of ξ_k is not shown along the paths $R \rightarrow M_1$ and $R \rightarrow M_2$. (Right panels) Dimensionless functions $c^{P/AP}(\varphi)$ that express the anisotropy of the ES around the Γ point as in equation (85). These are calculated from $\xi_k^{P/AP}$ along a circular path $\mathbf{k} = k(\cos \varphi, \sin \varphi)$ with $k = 0.001a/\ell^2$ and $\varphi \in [0, 2\pi]$. With proper rescaling, the curves for parallel and antiparallel fields coincide perfectly up to numerical precision, confirming the rescaling relation in equation (46). Namely, $(g_+/g_-)^{1/4}c^P(\varphi)$ and $(g_-/g_+)^{1/4}c^A(\varphi)$ share the same curves shown in black.

result in equation (50), we find that the data are well fitted by the form $S_e = \alpha_1 N_v - \alpha_2 \ln N_v + \alpha_3$ and that the coefficient α_2 obtained by the fitting is close to 1/4.

4.4. Fraction of depletion

Figure 9 shows numerical results on the fraction of depletion n'/n (scaled by ν^{-1}). As seen in figure 9(a), for an intercomponent repulsion (attraction), this quantity tends to be larger for parallel (antiparallel) fields, indicating stronger quantum fluctuations. This is in agreement with the field-theoretical result in equation (56). At the transition point between interlaced triangular and rhombic lattices, the fraction of depletion changes discontinuously owing to a discontinuous change in the lattice structure. Meanwhile, the fraction of depletion diverges at

both the transition points between rhombic, square, and rectangular lattices; this seems to be related to rapid changes in the inner angle and the aspect ratio in the mean-field ground state as shown in figure 11. In figure 9(b), we examine the scaling of $\nu n'/n$ as a function of N_v . The data are well fitted by the logarithmic form $\nu n'/n = \gamma_1 \ln N_v + \gamma_2$, in agreement with the field-theoretical result in equation (56).

4.5. Ground-state phase diagrams

Here we analyze how quantum fluctuations affect the ground-state phase diagrams for parallel and antiparallel fields. The GP mean-field analyses [36–39] have led to the five types of lattice structures that depend on $g_{\uparrow\downarrow}/g$ as shown in figure 1. We assume that the same types of structures appear in the

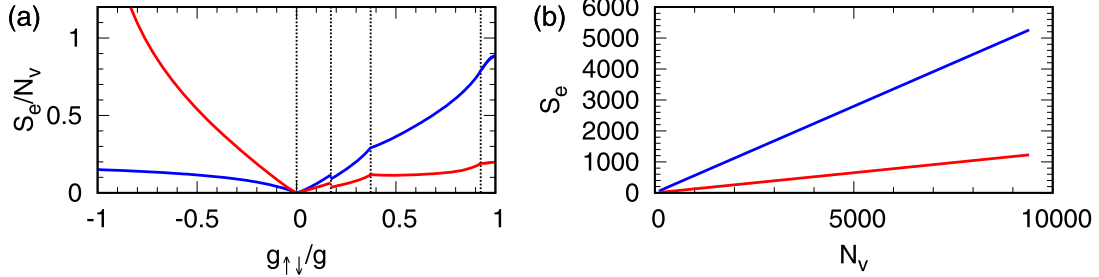


Figure 8. (a) Intercomponent EE per flux quantum, S_e/N_v , as a function of $g_{\uparrow\downarrow}/g$ for parallel (blue) and antiparallel (red) fields for $N_v = 97^2$. This is calculated from numerically obtained ξ_k using equation (81). Vertical dashed lines indicate the transition points. (b) Intercomponent EE S_e versus N_v for $g_{\uparrow\downarrow}/g = 0.75$. A fit to the form $S_e = \alpha_1 N_v - \alpha_2 \ln N_v + \alpha_3$ gives $(\alpha_1, \alpha_2, \alpha_3) = (0.560, 0.236, -0.70)$ for parallel fields and $(\alpha_1, \alpha_2, \alpha_3) = (0.130, 0.243, -0.06)$ for antiparallel fields.

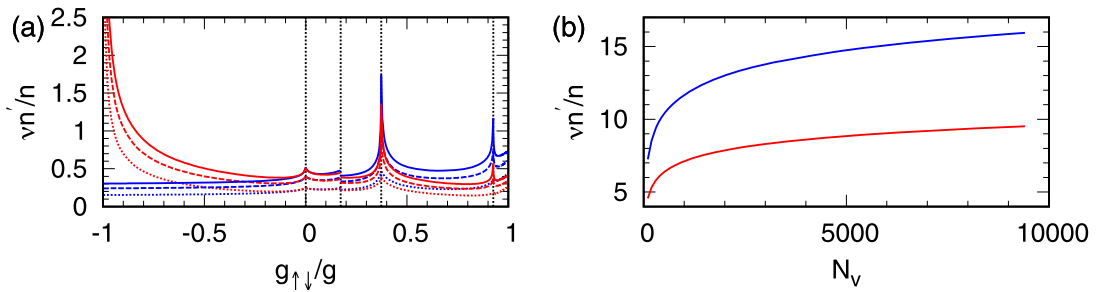


Figure 9. (a) Fraction of depletion n'/n (scaled by ν^{-1}) as a function of $g_{\uparrow\downarrow}/g$ for parallel (blue) and antiparallel (red) fields for $N_v = 5^2$ (dotted), 11^2 (dashed), and 19^2 (solid). The calculations are based on equation (69). Vertical dashed lines indicate the transition points. (b) $\nu n'/n$ versus N_v for $g_{\uparrow\downarrow}/g = 0.75$. A fit to the form $\nu n'/n = \gamma_1 \ln N_v + \gamma_2$ gives $(\gamma_1, \gamma_2) = (1.91, -1.53)$ for parallel fields and $(\gamma_1, \gamma_2) = (1.09, -0.40)$ for antiparallel fields.

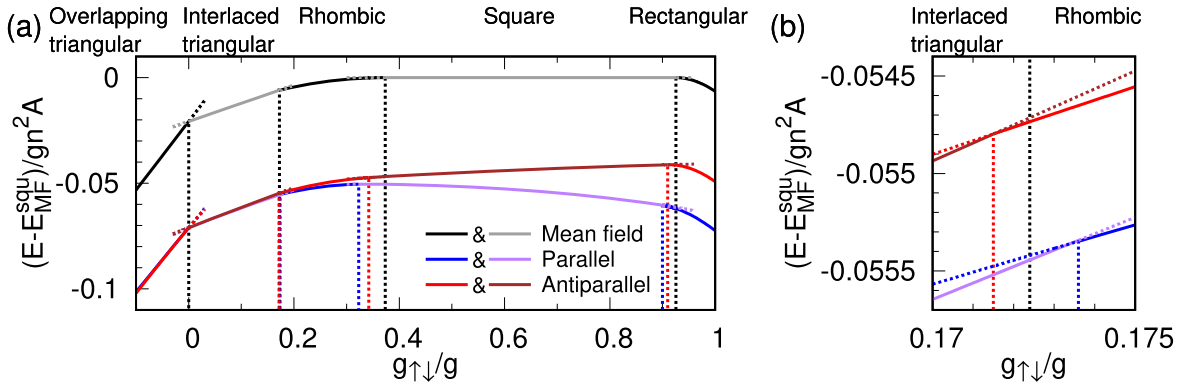


Figure 10. (a) Ground-state energy (equation (67)) as a function of $g_{\uparrow\downarrow}/g$. The mean-field energy (black and grey) is appreciably changed by a quantum correction, as shown for both parallel (blue and purple) and antiparallel (red and brown) fields for $\nu = 20$. The mean-field energy for the square lattices, $E_{MF}^{\text{SQU}} / (gn^2 A) = 1.180\,34 + 0.834\,627 g_{\uparrow\downarrow}/g$, is subtracted to emphasize the changes due to quantum fluctuations. Vertical dashed lines indicate the transition points, and alternating colors correspond to different phases. In particular, the transition points between rhombic-, square- and rectangular lattices shift appreciably owing to quantum corrections. In contrast, the transition point $g_{\uparrow\downarrow}/g = 0$ between overlapping and interlaced triangular lattices remain unchanged by quantum corrections. (b) Enlarged view of (a) around the transition point between interlaced triangular and rhombic lattices, which also shows small shifts due to quantum corrections.

presence of quantum fluctuations as well, and examine a quantum correction to the ground-state energy.

Figure 10 shows the mean-field ground-state energy as well as those with quantum corrections for parallel and antiparallel fields, where the filling factor is $\nu = 20$. Here, the energies for rhombic and rectangular lattices are minimized with respect to the inner angle θ and the aspect ratio b/a , respectively. As seen in figure 10(a), the transition points between rhombic, square and rectangular lattices shift appreciably owing

to quantum corrections; the shift occurs more significantly for parallel fields. In contrast, the transition point $g_{\uparrow\downarrow}/g = 0$ between overlapping and interlaced triangular lattices remains unchanged by quantum corrections. While the shift of the transition point between interlaced triangular and rhombic lattices is not clearly seen in figure 10(a), the shift indeed occurs as seen in the enlarged plot in figure 10(b).

Figures 11(a) and (b) show the inner angle θ of rhombic lattices and the aspect ratio b/a of rectangular lattices,

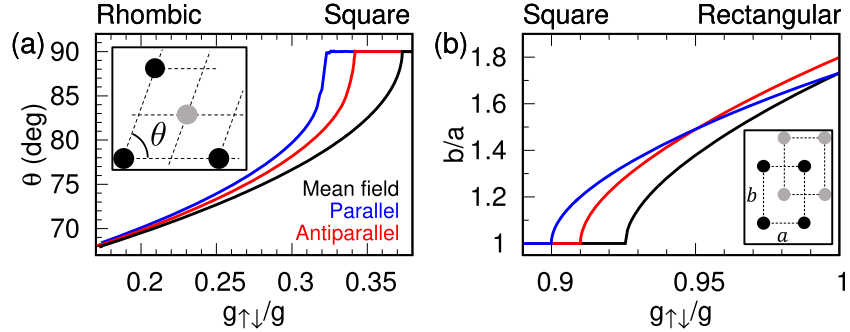


Figure 11. (a) The inner angle θ of rhombic lattices and (b) the aspect ratio b/a of rectangular lattices, plotted against $g_{\uparrow\downarrow}/g$. The mean-field results (black) [36] are changed appreciably by quantum corrections, as shown both for parallel (blue) and antiparallel (red) fields. Insets show the definitions of θ and b/a .

respectively, which are obtained through the one-parameter minimization of the ground-state energy (67). In the mean-field results, both the inner angle θ and the aspect ratio b/a show rapid changes near the transition points to square lattices [46]. In these regimes, the systems are expected to be highly susceptible to quantum fluctuations. Indeed, changes in θ and b/a are enhanced in these regimes, which explains the large shifts of the transition points as demonstrated in figure 10(a).

5. Summary and outlook

In this paper, we have presented a detailed comparative study of vortex lattices of binary BECs in parallel and antiparallel synthetic magnetic fields. Within the GP mean-field theory valid for high filling factors $\nu \gg 1$, the two types of fields are known to lead to the same phase diagram that consists of a variety of vortex lattices [36–39, 42]. We have formulated an improved effective field theory for such vortex lattices by introducing renormalized coupling constants for coarse-grained densities, and studied properties of collective modes and ground-state intercomponent entanglement. We have also performed numerical calculations based on the Bogoliubov theory with the LLL approximation to confirm the field-theoretical predictions. We have shown that the low-energy excitation spectra for the two types of fields are related to each other by suitable rescaling using the renormalized coupling constants (equations (36) and (37) and figures 4 and 5). By calculating the intercomponent EE in the ground state, we have found that for an intercomponent repulsion (attraction), the two components are more strongly entangled in the case of parallel (antiparallel) fields (equation (51) and figure 8(a)), in qualitative agreement with recent numerical results for a quantum (spin) Hall regime [42, 52]. As a by-product, we have also found that the ES exhibits an anomalous square-root dispersion relation (equation (43) and figure 7), and that the EE exhibits a volume-law scaling followed by a subleading logarithmic term (equation (50) and figure 8(b)). Finally, we have investigated the effects of quantum fluctuations on the phase diagrams by calculating the correction to the ground-state energy due to zero-point fluctuations in the Bogoliubov theory (equation (67) and figure 10).

We have found that the boundaries between rhombic-, square-, and rectangular-lattice phases shift appreciably with a decrease in ν .

We have found a similarity between the regimes of high ($\nu \gg 1$) and low ($\nu = O(1)$) filling factors in the behavior of intercomponent entanglement. It will be interesting to investigate how the two regimes are connected by applying sophisticated numerical methods such as a variational wave function [22] and the infinite density matrix renormalization group [51]. Furthermore, the similarity between the two regimes suggests that the behavior of intercomponent entanglement does not depend on the details of the systems and can be universal for a wide range of Hamiltonians. In fact, it has been found in lattice models that two coupled bosonic Laughlin states with opposite chiralities (i.e., fractional quantum spin Hall states [44]) are more robust against an intercomponent repulsion than the ones with the same chirality [79]. The stability of fractional quantum spin Hall states against an intercomponent repulsion has also been discussed in fermionic models [80–83]. Comparative investigation of multicomponent systems in gauge fields with different symmetries as in the present study will be a useful approach for exploring universal features of interacting topological states of matter.

Acknowledgments

TY is grateful to Kazuya Fujimoto, Yuki Kawaguchi, and Terumichi Ohashi for stimulating discussions during his stay at Nagoya University. This work was supported by KAKENHI Grant Nos. JP18H01145 and JP18K03446, a Grant-in-Aid for Scientific Research on Innovative Areas ‘Topological Materials Science’ (KAKENHI Grant No. JP15H05855) from the Japan Society for the Promotion of Science (JSPS), and Keio Gijuku Academic Development Funds. TY was supported by JSPS through the Program for Leading Graduate School (ALPS).

Data availability statement

All data that support the findings of this study are included within the article (and any supplementary files).

Appendix A. Entanglement spectrum and entanglement Hamiltonian

Here we describe details of the calculation of the ES $\xi_{\mathbf{k}}$ and the coefficients $F_{\mathbf{k}}$ and $G_{\mathbf{k}}$ in the entanglement Hamiltonian in section 2.5.

For preparation, we calculate the phase and density correlators in the oscillator ground state $|0^{\text{osc}}\rangle$ of the total system. By using equations (21), (25), and (29), the phase and the density of the spin- \uparrow component are expressed in terms of the bogolon operators as

$$\begin{aligned}\theta_{\mathbf{k},\uparrow} &= \frac{1}{2} (r_{\mathbf{k}}, r_{\mathbf{k}}^{-1}) U(\mathbf{k}) \begin{pmatrix} \bar{\theta}_{\mathbf{k},1} \\ \bar{\theta}_{\mathbf{k},2} \end{pmatrix} = \frac{1}{2} \sum_{j=1,2} R_{\mathbf{k},j} \bar{\theta}_{\mathbf{k},j} \\ &= \frac{1}{2\sqrt{2n}} \sum_{j=1,2} R_{\mathbf{k},j} \zeta_{\mathbf{k},j}^{-1} \left(\gamma_{\mathbf{k},j} + \gamma_{-\mathbf{k},j}^{\dagger} \right),\end{aligned}\quad (\text{A.1a})$$

$$\begin{aligned}n_{\mathbf{k},\uparrow} &= (r_{\mathbf{k}}^{-1}, r_{\mathbf{k}}) U(\mathbf{k}) \begin{pmatrix} \bar{n}_{\mathbf{k},1} \\ \bar{n}_{\mathbf{k},2} \end{pmatrix} = \sum_{j=1,2} R_{\mathbf{k},3-j} \bar{n}_{\mathbf{k},j} \\ &= \frac{1}{i} \sqrt{\frac{n}{2}} \sum_{j=1,2} R_{\mathbf{k},3-j} \zeta_{\mathbf{k},j} \left(\gamma_{\mathbf{k},j} - \gamma_{-\mathbf{k},j}^{\dagger} \right).\end{aligned}\quad (\text{A.1b})$$

Here we introduce

$$R_{\mathbf{k},1} := r_{\mathbf{k}} \cos \frac{\chi_{\mathbf{k}}}{2} + i r_{\mathbf{k}}^{-1} \sin \frac{\chi_{\mathbf{k}}}{2},\quad (\text{A.2a})$$

$$R_{\mathbf{k},2} := r_{\mathbf{k}}^{-1} \cos \frac{\chi_{\mathbf{k}}}{2} + i r_{\mathbf{k}} \sin \frac{\chi_{\mathbf{k}}}{2},\quad (\text{A.2b})$$

which satisfy $R_{-\mathbf{k},j} = R_{\mathbf{k},j}^*$ ($j = 1, 2$). As $|0^{\text{osc}}\rangle$ is the vacuum for bogolons, i.e., $\gamma_{\mathbf{k},\pm} |0^{\text{osc}}\rangle = 0$ for all $\mathbf{k} \neq \mathbf{0}$, the correlators of the operators in equation (A.1) are calculated as

$$\begin{aligned}\langle 0^{\text{osc}} | \theta_{-\mathbf{k},\uparrow} \theta_{\mathbf{k},\uparrow} | 0^{\text{osc}} \rangle &= \frac{1}{8n} \sum_{j=1,2} |R_{\mathbf{k},j}|^2 \zeta_{\mathbf{k},j}^{-2} \\ &= \frac{1}{8n\zeta_{\mathbf{k},1}\zeta_{\mathbf{k},2}} \left(|R_{\mathbf{k},1}|^2 \frac{\zeta_{\mathbf{k},2}}{\zeta_{\mathbf{k},1}} + |R_{\mathbf{k},2}|^2 \frac{\zeta_{\mathbf{k},1}}{\zeta_{\mathbf{k},2}} \right),\end{aligned}\quad (\text{A.3a})$$

$$\begin{aligned}\langle 0^{\text{osc}} | n_{-\mathbf{k},\uparrow} n_{\mathbf{k},\uparrow} | 0^{\text{osc}} \rangle &= \frac{n}{2} \sum_{j=1,2} |R_{\mathbf{k},3-j}|^2 \zeta_{\mathbf{k},j}^2 \\ &= \frac{n\zeta_{\mathbf{k},1}\zeta_{\mathbf{k},2}}{2} \left(|R_{\mathbf{k},1}|^2 \frac{\zeta_{\mathbf{k},2}}{\zeta_{\mathbf{k},1}} + |R_{\mathbf{k},2}|^2 \frac{\zeta_{\mathbf{k},1}}{\zeta_{\mathbf{k},2}} \right).\end{aligned}\quad (\text{A.3b})$$

We now require that the correlators (42) obtained from the Gaussian ansatz (38) be equal to the ones (A.3) obtained for the oscillator ground state $|0^{\text{osc}}\rangle$. We then find

$$\begin{aligned}f_B(\xi_{\mathbf{k}}) + \frac{1}{2} &= \sqrt{\langle 0^{\text{osc}} | \theta_{-\mathbf{k},\uparrow} \theta_{\mathbf{k},\uparrow} | 0^{\text{osc}} \rangle \langle 0^{\text{osc}} | n_{-\mathbf{k},\uparrow} n_{\mathbf{k},\uparrow} | 0^{\text{osc}} \rangle} \\ &= \frac{1}{4} \left(|R_{\mathbf{k},1}|^2 \frac{\zeta_{\mathbf{k},2}}{\zeta_{\mathbf{k},1}} + |R_{\mathbf{k},2}|^2 \frac{\zeta_{\mathbf{k},1}}{\zeta_{\mathbf{k},2}} \right),\end{aligned}\quad (\text{A.4a})$$

$$\sqrt{\frac{F_{\mathbf{k}}}{G_{\mathbf{k}}}} = \frac{1}{n} \sqrt{\frac{\langle 0^{\text{osc}} | n_{-\mathbf{k},\uparrow} n_{\mathbf{k},\uparrow} | 0^{\text{osc}} \rangle}{\langle 0^{\text{osc}} | \theta_{-\mathbf{k},\uparrow} \theta_{\mathbf{k},\uparrow} | 0^{\text{osc}} \rangle}} = 2\zeta_{\mathbf{k},1}\zeta_{\mathbf{k},2}.\quad (\text{A.4b})$$

In the long-wavelength limit $k\ell \ll 1$, we have

$$\begin{aligned}\zeta_{\mathbf{k},1} &\approx \left[\frac{gD(\varphi)}{2\bar{g}_{\pm}} \right]^{1/4} \sqrt{k\ell}, \quad \zeta_{\mathbf{k},2} \approx \left[\frac{gC(\varphi)}{2\bar{g}_{\mp}} \right]^{1/4} k\ell, \\ \cos \chi_{\mathbf{k}} &\approx \mp 1, \\ |R_{\mathbf{k},1}|^2 &= r_{\mathbf{k}}^2 \frac{1 + \cos \chi_{\mathbf{k}}}{2} + r_{\mathbf{k}}^{-2} \frac{1 - \cos \chi_{\mathbf{k}}}{2} \approx r_{\mathbf{0}}^{\pm 2} = \sqrt{\frac{\bar{g}_{\mp}}{\bar{g}_{\pm}}}, \\ |R_{\mathbf{k},2}|^2 &= r_{\mathbf{k}}^{-2} \frac{1 + \cos \chi_{\mathbf{k}}}{2} + r_{\mathbf{k}}^2 \frac{1 - \cos \chi_{\mathbf{k}}}{2} \approx r_{\mathbf{0}}^{\pm 2} = \sqrt{\frac{\bar{g}_{\pm}}{\bar{g}_{\mp}}},\end{aligned}\quad (\text{A.5})$$

where equation (32) is used. Then, $f_B(\xi_{\mathbf{k}})$ and $\sqrt{F_{\mathbf{k}}/G_{\mathbf{k}}}$ in equation (A.4) are calculated as

$$f_B(\xi_{\mathbf{k}}) \approx \frac{1}{4} \left[\frac{\bar{g}_{\pm} D(\varphi)}{\bar{g}_{\mp} C(\varphi)} \right]^{1/4} (k\ell)^{-1/2},\quad (\text{A.6a})$$

$$\sqrt{\frac{F_{\mathbf{k}}}{G_{\mathbf{k}}}} \approx \left[\frac{4g^2 C(\varphi) D(\varphi)}{\bar{g}_{+} \bar{g}_{-}} \right]^{1/4} (k\ell)^{3/2},\quad (\text{A.6b})$$

from which we obtain equation (43).

Appendix B. Phase correlation function

Here we describe the derivation of the phase correlation function (54). Using equation (52), this correlation function is expressed as

$$\langle [\theta_{\uparrow}(\mathbf{r}) - \theta_{\uparrow}(\mathbf{0})]^2 \rangle \approx \frac{2}{nF\ell^2} [G(\mathbf{0}; \alpha) - G(\mathbf{r}; \alpha)].\quad (\text{B.1})$$

Here, $G(\mathbf{r}; \alpha)$ is Green's function for the 2D Poisson equation

$$G(\mathbf{r}; \alpha) = \frac{1}{A} \sum_{\mathbf{k} \neq \mathbf{0}} \frac{1}{k^2} e^{-\alpha k + i\mathbf{k} \cdot \mathbf{r}} = \frac{1}{A} \sum_{\mathbf{k} \neq \mathbf{0}} \frac{1}{k^2} e^{-\alpha k + ikr \cos \theta},\quad (\text{B.2})$$

where we express the wave vector \mathbf{k} in terms of the polar coordinate (k, θ) with θ being the angle relative to \mathbf{r} . Although the logarithmic behavior of Green's function for the 2D Poisson

equation is known, we derive it within the present regularization scheme using the convergence factor $e^{-\alpha k}$.

By differentiating equation (B.2) with respect to r , we have

$$\begin{aligned} -\frac{\partial}{\partial r} G(\mathbf{r}; \alpha) &= \frac{1}{A} \sum_{\mathbf{k} \neq 0} \frac{-i \cos \theta}{k} e^{-\alpha k + ikr \cos \theta} \\ &= \frac{1}{(2\pi)^2} \int_0^{2\pi} d\theta \int_0^\infty dk (-i \cos \theta) e^{-k(\alpha - ir \cos \theta)} \\ &= \frac{1}{(2\pi)^2} \int_0^{2\pi} d\theta \frac{-i \cos \theta}{\alpha - ir \cos \theta}. \end{aligned} \quad (\text{B.3})$$

With a change of the integration variable as $z = e^{i\theta}$, the last integral in equation (B.3) can be written as a contour integral along the unit circle:

$$\begin{aligned} -\frac{\partial}{\partial r} G(\mathbf{r}; \alpha) &= \frac{1}{(2\pi)^2} \oint \frac{dz}{iz} \frac{z^2 + 1}{r(z^2 + 1) + 2i\alpha z} \\ &= \frac{1}{(2\pi)^2 ir} \oint dz \frac{z^2 + 1}{z(z - z_+)(z - z_-)}, \end{aligned} \quad (\text{B.4})$$

where $z_\pm = i(-\alpha \pm \sqrt{r^2 + \alpha^2})/r$ are the locations of poles. Since $|z_+| < 1 < |z_-|$, the integral picks up the residues at $z = 0$ and z_+ , leading to

$$\begin{aligned} -\frac{\partial}{\partial r} G(\mathbf{r}; \alpha) &= \frac{1}{2\pi r} \left[\frac{1}{z_+ z_-} + \frac{z_+^2 + 1}{z_+ (z_+ - z_-)} \right] \\ &= \frac{1}{2\pi r} \left(1 - \frac{\alpha}{\sqrt{r^2 + \alpha^2}} \right). \end{aligned} \quad (\text{B.5})$$

Therefore, $G(\mathbf{0}; \alpha) - G(\mathbf{r}; \alpha)$ in equation (B.1) can be calculated as

$$\begin{aligned} G(\mathbf{0}; \alpha) - G(\mathbf{r}; \alpha) &= \frac{1}{2\pi} \lim_{a_0 \rightarrow 0} \int_{a_0}^r dr' \left(\frac{1}{r'} - \frac{\alpha}{r' \sqrt{r'^2 + \alpha^2}} \right) \\ &= \frac{1}{2\pi} \lim_{a_0 \rightarrow 0} \left(\ln \frac{r}{a_0} + \text{arsinh} \frac{\alpha}{r} - \text{arsinh} \frac{\alpha}{a_0} \right) \\ &= \frac{1}{2\pi} \left(\ln \frac{r}{2\alpha} + \text{arsinh} \frac{\alpha}{r} \right). \end{aligned} \quad (\text{B.6})$$

By substituting this into equation (B.1) and taking the limit $r \gg \alpha$, we obtain equation (54).

ORCID iDs

Shunsuke Furukawa  <https://orcid.org/0000-0003-3376-7198>

Masahito Ueda  <https://orcid.org/0000-0002-5367-1436>

References

- [1] Dalibard J, Gerbier F, Juzeliūnas G and Öhberg P 2011 *Rev. Mod. Phys.* **83** 1523
- [2] Goldman N, Juzeliūnas G, Öhberg P and Spielman I B 2014 *Rep. Prog. Phys.* **77** 126401
- [3] Zhang S-L and Zhou Q 2017 *J. Phys. B: At. Mol. Opt. Phys.* **50** 222001
- [4] Aidelsburger M, Nascimbene S and Goldman N 2018 *C. R. Phys.* **19** 394–432
- [5] Galitski V, Juzeliūnas G and Spielman I B 2019 *Phys. Today* **72** 38–44
- [6] Cooper N R 2008 *Adv. Phys.* **57** 539
- [7] Fetter A L 2009 *Rev. Mod. Phys.* **81** 647
- [8] Lin Y-J, Compton R L, Jiménez-García K, Porto J V and Spielman I B 2009 *Nature* **462** 628
- [9] Abrikosov A A 1957 *Sov. Phys. JETP* **5** 1174
Abrikosov A A 1957 *Zh. Eksp. Teor. Fiz.* **32** 1442
- [10] Abo-Shaeer J R, Raman C, Vogels J M and Ketterle W 2001 *Science* **292** 476
- [11] Engels P, Coddington I, Haljan P C and Cornell E A 2002 *Phys. Rev. Lett.* **89** 100403
- [12] Schweikhard V, Coddington I, Engels P, Mogendorff V P and Cornell E A 2004 *Phys. Rev. Lett.* **92** 040404
- [13] Tkachenko V K 1966 *Sov. Phys. JETP* **22** 1282
Tkachenko V K 1966 *Zh. Eksp. Teor. Fiz.* **49** 1875
- [14] Tkachenko V K 1966 *Sov. Phys. JETP* **23** 1049
Tkachenko V K 1966 *Zh. Eksp. Teor. Fiz.* **50** 1573
- [15] Tkachenko V K 1969 *Sov. Phys. JETP* **29** 945
Tkachenko V K 1969 *Zh. Eksp. Teor. Fiz.* **56** 1763
- [16] Sonin E B 1987 *Rev. Mod. Phys.* **59** 87
- [17] Coddington I, Engels P, Schweikhard V and Cornell E A 2003 *Phys. Rev. Lett.* **91** 100402
- [18] Sinova J, Hanna C B and MacDonald A H 2002 *Phys. Rev. Lett.* **89** 030403
- [19] Baym G 2003 *Phys. Rev. Lett.* **91** 110402
- [20] Baym G 2004 *Phys. Rev. A* **69** 043618
- [21] Matveenko S I and Shlyapnikov G V 2011 *Phys. Rev. A* **83** 033604
- [22] Kwasigroch M P and Cooper N R 2012 *Phys. Rev. A* **86** 063618
- [23] Watanabe H and Murayama H 2013 *Phys. Rev. Lett.* **110** 181601
- [24] Ho T L 2001 *Phys. Rev. Lett.* **87** 060403
- [25] Sonin E B 2005 *Phys. Rev. A* **72** 021606
- [26] Wilkin N K, Gunn J M F and Smith R A 1998 *Phys. Rev. Lett.* **80** 2265
- [27] Cooper N R, Wilkin N K and Gunn J M F 2001 *Phys. Rev. Lett.* **87** 120405
- [28] Cooper N R 2020 *Fractional Quantum Hall Effects* ed B I Halperin and J K Jain (Singapore: World Scientific)
- [29] Cooper N R and Rezayi E H 2007 *Phys. Rev. A* **75** 013627
- [30] Liu Z, Guo H L, Vedral V and Fan H 2011 *Phys. Rev. A* **83** 013620
- [31] Schweikhard V, Coddington I, Engels P, Tung S and Cornell E A 2004 *Phys. Rev. Lett.* **93** 210403
- [32] Lin Y-J, Jiménez-García K and Spielman I B 2011 *Nature* **471** 83
- [33] Zhai H 2012 *Int. J. Mod. Phys. B* **26** 1230001
- [34] Wu Z et al 2016 *Science* **354** 83–8
- [35] Beeler M C, Williams R A, Jiménez-García K, LeBlanc L J, Perry A R and Spielman I B 2013 *Nature* **498** 201
- [36] Mueller E J and Ho T-L 2002 *Phys. Rev. Lett.* **88** 180403
- [37] Kasamatsu K, Tsubota M and Ueda M 2003 *Phys. Rev. Lett.* **91** 150406
- [38] Kasamatsu K, Tsubota M and Ueda M 2005 *Int. J. Mod. Phys. B* **19** 1835
- [39] Mingarelli L, Keaveny E E and Barnett R 2018 *Phys. Rev. A* **97** 043622
- [40] Liu X J, Liu X, Kwek L C and Oh C H 2007 *Phys. Rev. Lett.* **98** 026602
- [41] Fialko O, Brand J and Zülicke U 2014 *New J. Phys.* **16** 025006
- [42] Furukawa S and Ueda M 2014 *Phys. Rev. A* **90** 033602
- [43] Girvin S M and MacDonald A H 1997 *Perspectives in Quantum Hall Effects* ed S Das Sarma and A Pinczuk (New York: Wiley)

[44] Bernevig B A and Zhang S-C 2006 *Phys. Rev. Lett.* **96** 106802

[45] Keçeli M and Oktel M O 2006 *Phys. Rev. A* **73** 023611

[46] Yoshino T, Furukawa S, Higashikawa S and Ueda M 2019 *New J. Phys.* **21** 015001

[47] Furukawa S and Ueda M 2013 *Phys. Rev. Lett.* **111** 090401

[48] Wu Y-H and Jain J K 2013 *Phys. Rev. B* **87** 245123

[49] Regnault N and Senthil T 2013 *Phys. Rev. B* **88** 161106

[50] Wu Y H and Jain J K 2015 *Phys. Rev. A* **91** 063623

[51] Geraedts S D, Repellin C, Wang C, Mong R S K, Senthil T and Regnault N 2017 *Phys. Rev. B* **96** 075148

[52] Furukawa S and Ueda M 2017 *Phys. Rev. A* **96** 053626

[53] Woo S J, Choi S, Baksmaty L O and Bigelow N P 2007 *Phys. Rev. A* **75** 031604

[54] Barnett R, Refael G, Porter M A and Büchler H P 2008 *New J. Phys.* **10** 043030

[55] Mason P and Aftalion A 2011 *Phys. Rev. A* **84** 033611

[56] Aftalion A, Mason P and Wei J 2012 *Phys. Rev. A* **85** 033614

[57] Kuopanportti P, Huhtamäki J A M and Möttönen M 2012 *Phys. Rev. A* **85** 043613

[58] Kumar R K, Tomio L, Malomed B A and Gammal A 2017 *Phys. Rev. A* **96** 063624

[59] Mingarelli L and Barnett R 2019 *Phys. Rev. Lett.* **122** 045301

[60] Lee T D, Huang K and Yang C N 1957 *Phys. Rev.* **106** 1135–45

[61] Yoshino T, Furukawa S and Ueda M 2021 *Phys. Rev. A* **103** 043321

[62] Chen X and Fradkin E 2013 *J. Stat. Mech.* P08013

[63] Lundgren R, Fuji Y, Furukawa S and Oshikawa M 2013 *Phys. Rev. B* **88** 245137

[64] Moroz S, Hoyos C, Benzoni C and Son D T 2018 *SciPost Phys.* **5** 039

[65] Moroz S and Son D T 2019 *Phys. Rev. Lett.* **122** 235301

[66] Aftalion A, Blanc X and Dalibard J 2005 *Phys. Rev. A* **71** 023611

[67] Peschel I 2003 *J. Phys. A: Math. Gen.* **36** L205–8

[68] Peschel I and Eisler V 2009 *J. Phys. A: Math. Theor.* **42** 504003

[69] Metlitski M A and Grover T 2011 Entanglement entropy of systems with spontaneously broken continuous symmetry (arXiv:1112.5166)

[70] Pethick C J and Smith H 2008 *Bose–Einstein Condensation in Dilute Gases* 2nd edn (Cambridge: Cambridge University Press)

[71] Penrose O and Onsager L 1956 *Phys. Rev.* **104** 576–84

[72] Yang C N 1962 *Rev. Mod. Phys.* **34** 694–704

[73] Rashba E I, Zhukov L E and Efros A L 1997 *Phys. Rev. B* **55** 5306

[74] Burkov A A 2010 *Phys. Rev. B* **81** 125111

[75] Panfilov I, Patri A, Yang K and Burkov A A 2016 *Phys. Rev. B* **93** 125126

[76] Furukawa S and Kim Y B 2011 *Phys. Rev. B* **83** 085112

[77] Xu C 2011 *Phys. Rev. B* **84** 125119

[78] Mollabashi A, Shiba N and Takayanagi T 2014 *J. High Energy Phys.* JHEP04(2014)085

[79] Repellin C, Bernevig B A and Regnault N 2014 *Phys. Rev. B* **90** 245401

[80] Neupert T, Santos L, Ryu S, Chamon C and Mudry C 2011 *Phys. Rev. B* **84** 165107

[81] Li W, Sheng D N, Ting C S and Chen Y 2014 *Phys. Rev. B* **90** 081102

[82] Chen H and Yang K 2012 *Phys. Rev. B* **85** 195113

[83] Ghaemi P, Cayssol J, Sheng D N and Vishwanath A 2012 *Phys. Rev. Lett.* **108** 266801